Geotech Geol Eng (2026) 44:45
https://doi.org/10.1007/s10706-025-03574-5

ORIGINAL PAPER

Microwave Convective Drying and Predictive Modelling of Compacted Unbound Granular Materials

Gopoojithaa Athmarajah · Amir Tophel · Jeffrey P. Walker · Jayantha Kodikara

Received: 5 November 2025 / Accepted: 4 December 2025 / Published online: 17 December 2025

Abstract Drying of wet unbound granular pavement layers to a lower moisture content or degree of saturation (S_r) after compaction is one of the important processes in road construction. The efficiency of this so-called dry-back process is crucial for ensuring pavement stability before primer sealing. Traditional drying methods rely on solar radiation, which is slow and weather-dependent, leading to delays in construction timelines. Consequently, microwave drying has been explored as a rapid alternative; however, its effectiveness is limited by non-uniform moisture removal and shallow penetration depth (~50—60 mm). Hence, this study investigated the potential of microwave convective drying, integrating microwave energy with hot airflow to enhance the drying efficiency of a compacted unbound granular material (UGM). Laboratory-scale experiments were conducted to assess the influence of air temperature, airflow speed, airflow angle, and drying duration on moisture removal. Results showed that microwave convective drying improved surface drying efficiency compared to microwave drying alone, as evidenced by a larger dried area and wider surface temperature distribution. Nevertheless, both approaches exhibited similar limitations in deeper moisture removal, resulting in non-uniform drying. Two machine learning models, Support Vector Machine (SVM) and Gaussian Process Regression (GPR), were trained to predict the final S_r based on experimental data. The models predicted the drying trends reasonably well, with SVM yielding a mean absolute error (MAE) of 0.924% and GPR producing 0.006% in terms of S_r ratio. These findings highlight the benefits and limitations of microwave convective drying, suggesting the need for further optimisation for road construction applications.

Keywords Microwave convective drying · Degree of saturation · Temperature · Hot airflow · UGM

Abbreviations

UGM	Unbound granular material
S_r	Degree of saturation (%)
OMC	Optimum moisture content (w/w) (%)
MDD	Maximum dry density (kg/m^3)
SVM	Support vector machine

G. Athmarajah · J. P. Walker · J. Kodikara
ARC Industrial Transformation Research Hub (ITRH) – SPARC Hub, Dept. of Civil and Environmental Engineering, Monash University, Clayton Campus VIC 3800, Australia
e-mail: gopoojithaa.athmarajah@monash.edu

J. P. Walker
e-mail: jeff.walker@monash.edu

J. Kodikara
e-mail: Kodikarajayantha.kodikara@monash.edu

A. Tophel (✉)
ARC Industrial Transformation Research Hub (ITRH) – SPARC Hub, Department of Civil and Environmental Engineering, Monash University, Clayton Campus VIC 3800, Australia
e-mail: amir.tophel@monash.edu

GPR	Gaussian process regression
MAE	Mean absolute error
R^2	Coefficient of determination
RMSE	Root mean square error

1 Introduction

Unbound granular material (UGM), primarily composed of crushed rock or gravel with a sufficient proportion of fines, is widely used in the base and subbase layers of road construction. In Australia, UGM forms the foundation of approximately 90% of the road network, covered with a thin seal (Austroads 2019). Their widespread use in road infrastructure is attributed to their natural availability, mechanical strength and cost-effectiveness, making them a preferred choice for flexible pavement design (Griffin 2015; Dutta et al. 2024). This UGM is compacted at or near its optimum moisture content (OMC) to achieve maximum dry density (MDD) for a given compaction effort. After compaction, the wet UGM layers are allowed to dry back to a lower moisture condition before primer sealing, ensuring pavement stability and longevity. A high moisture level in the compacted UGM layer can lead to a reduction in shear strength, loss of stiffness, and poor load-bearing capacity, ultimately resulting in rutting and premature pavement failure (Sun et al. 2021; Sangsefidi et al. 2019; Maha Madakalapuge et al. 2024; Salour 2015; Tophel et al. 2023b). Additionally, sufficient dry-back of the UGM layers provides better resistance to the embedment of sealing aggregate into moist pavement layers (Midgley 2010; Kodikara et al. 2018).

In current practice, the dry-back process relies on solar radiation, which is highly dependent on weather conditions, making it time-consuming and unpredictable (Athmarajah et al. 2023). Delays in achieving the required moisture levels can prolong construction timelines and incur additional costs (Kukkapalli and Pulugurtha 2018). To address this challenge, microwave technology has been proposed as an alternative method to accelerate the dry-back process by rapidly heating and removing moisture from a compacted UGM (Athmarajah et al. 2025).

Microwave drying has been widely explored across various applications: food processing, ceramics, wood, pharmaceuticals and soil remediation, due to its unique heating mechanism (Yao et al. 2020; Brodie et al. 2019b, 2020; Li et al. 2024; Himanshu et al. 2010). Unlike conventional drying methods that rely on surface heat transfer, microwave energy penetrates the material and generates heat internally, leading to faster moisture removal (Ulloa et al. 2019). However, microwave drying of compacted UGM presents a unique challenge. Earlier experimental investigations on microwave drying by Athmarajah (2025) showed that the depth of effective energy penetration is limited to approximately 50—60 mm from the surface. This shallow penetration results from the dependence of dielectric properties on moisture content and temperature, which may reduce energy absorption in deeper layers as drying progresses (Athmarajah et al. 2024). In contrast, the thickness of the compacted unbound granular pavement layers typically ranges from 75 to 250 mm, depending on road authority regulations and material type (Department of Transport and Main Roads Queensland, 2021). These findings highlight that microwave drying, although effective at rapid heating near the surface, poses practical limitations when applied to full-thickness pavement layers.

Convective drying, a well-established method, facilitates the removal of moisture through the movement of hot air, which transfers heat and mass to and from the surface of a material. This method has been widely used in various industries such as food processing, wood, textiles and weed control (Deb et al. 2024; Brodie 2005; Domínguez 2011; Sousa et al. 2006). Further, many researchers have investigated the benefits of combining microwave and convective drying (Malafronte et al. 2012; Kumar et al. 2017), with this hybrid approach applied to a range of products, including foods, ceramics, and wood. In these materials, convective heating has been shown to improve heat transfer and promote surface evaporation, leading to faster moisture removal in porous materials (Li et al. 2023; Izli et al. 2022; Ouertani et al. 2015; Rajewska and Pawłowski 2018). Despite these demonstrated benefits, microwave convective drying has not yet been applied to a compacted UGM, and its potential to address the limitations observed in microwave drying remains unexplored.

Given the limited penetration depth of microwave drying and the need for more uniform drying in pavement applications, this study has investigated the suitability of using microwave convective drying, which is the combination of microwave energy with a controlled hot airflow to enhance drying efficiency.

Laboratory-scale experiments were performed to evaluate the impact of key parameters: air temperature, airflow speed, airflow angle, and drying duration on the drying behaviour of a compacted UGM, comparing results with microwave drying alone. This preliminary investigation provides essential insight into the fundamental drying response of UGM and the feasibility of this hybrid method for field applications.

Recent studies in geotechnical engineering have explored the application of machine learning models for predictive analysis, due to their ability to capture complex nonlinear behaviour and work effectively with limited datasets (Zhang et al. 2022; Tophel et al. 2023a; Elsawy et al. 2022; Shao et al. 2023; Arif et al. 2025). In this study, predictive models using Support Vector Machine (SVM) and Gaussian Process Regression (GPR) were developed to assess drying performance under varying experimental conditions. By systematically analysing experimental data and employing machine learning techniques, this study aimed to provide foundational insights into the potential advantages and limitations of microwave convective drying, addressing a key gap in current research and supporting future development of accelerated dry-back strategies for pavement construction.

2 Machine Learning Approaches

2.1 Support Vector Machine (SVM) Model

SVM is a powerful supervised learning algorithm used for classification and regression tasks (Cristianini and Shawe-Taylor 2000; Tophel et al. 2023a). It works by finding the hyperplane that best separates the data points in a high-dimensional space (Pan et al. 2025). In regression, known as Support Vector Regression (SVR), SVM aims to find a function that approximates target values within a certain margin of tolerance, defined by a parameter epsilon, ε (Smola and Schölkopf 2004). SVM regression works by identifying the optimal hyperplane in a high-dimensional space that minimises prediction error while ensuring robustness. The optimisation problem for SVM is thus formulated as (Awad and Khanna 2015)

$$\min_{w,b,\xi,\xi^*} \frac{1}{2}\|w\|^2 + C\sum_{i=1}^{n}\left(\xi_i + \xi_i^*\right), \tag{1}$$

subject to

$$y_i - \left(w.\phi\left(x_i\right) + b\right) \le \left(\varepsilon + \xi_i\right), \tag{2}$$

$$\left(w.\phi\left(x_i\right) + b\right) - y_i \le \left(\varepsilon + \xi_i^*\right), \tag{3}$$

where $\boldsymbol{w}$ is the weight vector, b is the bias term, ξ_i and ξ_i^* are slack variables (ξ_i and $\xi_i^* \ge 0$), C is the box constraint that controls the trade-off between achieving a low training error and low testing error, x and y are respectively the input and output response values, and $\phi(x)$ is the kernel function that maps the input features into a higher-dimensional space. The kernel function $\phi(x)$ plays a critical role in transforming the input space. In this study, a polynomial kernel was chosen which can be represented as

$$\phi(x) = \left(\gamma x.x' + r\right)^d, \tag{4}$$

where γ is the kernel scale, r is a coefficient and d is the degree of the polynomial. In this study, the SVM approach was chosen for its ability to handle nonlinear relationships in the data, making it suitable for predicting the complex drying behaviour of a UGM.

2.2 Gaussian Process Regression (GPR) Model

GPR is a non-parametric Bayesian approach used for regression analysis to provide a probabilistic prediction model (Rasmussen and Williams 2006; Williams and Rasmussen 1996). It assumes that the underlying function to be predicted is drawn from a Gaussian process, defined by a mean function $m(x)$, and a covariance function (kernel, $k(x)$) such that (Chaure et al. 2023)

$$f(x) \sim \mathrm{GP}(m(x), k(x)). \tag{5}$$

The covariance function determines the smoothness and correlation of the function over the input space, making GPR beneficial for capturing uncertainties and modelling complex relationships. In this study, the Matern kernel was used as the covariance function which can be represented by (Dai et al. 2023)

$$k(x) = \sigma^2 \frac{2^{1-\upsilon}}{\Gamma(\upsilon)}\left(\sqrt{2\upsilon}\frac{r}{l}\right)^{\upsilon} K_{\upsilon}\left(\sqrt{2\upsilon}\frac{r}{l}\right), \tag{6}$$

where $r = |x - x'|$ is the Euclidean distance between x and $x\prime$,x is the current input parameter, $x\prime$ is another input with which x is being compared, l is the length scale that determines the smoothness of the predicted function, σ is the standard deviation that controls the vertical variation of the function, Γ is the gamma function, K_υ is the modified Bessel function, and υ is usually set equal to 3/2 (matern32) or 5/2 (matern52). In this study, GPR was selected for its robustness in providing reliable predictions and its ability to quantify uncertainty, which is crucial for understanding the variability in the drying behaviour of a UGM.

3 Methodology

3.1 Material Properties and Sample Preparation

A Class 2 UGM, as classified according to Australian guidelines (VicRoads 2017), was chosen for this study because it is commonly used in base and subbase construction in Australia. Figure 1 illustrates the particle size distribution of the chosen UGM. The geotechnical properties of the selected material are detailed in Table 1.

The selected UGM was oven-dried at 105 ℃ for 24 h. Subsequently, the dried UGM was mixed with water to achieve the target moisture content for compaction. The UGM samples were compacted at gravimetric moisture contents ranging from 5.1% to 5.9%, closer to the OMC of 5.7%, to simulate the field compaction practices. To ensure moisture

Table 1 Geotechnical properties of the selected unbound granular materials (Class 2)

Geotechnical property	Value	Standard
MDD, modified [kg/m^3]	2345	[AS-1289.5.2.1, 2017]
OMC, modified[(w/w), %]	5.7	[AS-1289.5.2.1, 2017]
Optimum degree of saturation [$S_{r,opt}$, %]	85	[AS-1289.5.2.1, 2017]
Specific gravity [G_s, g/g]	2.78	[AS-1289.3.5.1, 2006]
Liquid limit [LL, %]	22	[AS-1289.3.1.1, 2009]
Plastic limit [PL, %]	17.5	[AS-1289.3.1.1, 2009]
Plastic index [PI, %]	4.5	[AS-1289.3.1.1, 2009]
Fine percentage [%]	10.4	[AS-1289.3.6.1, 2009]

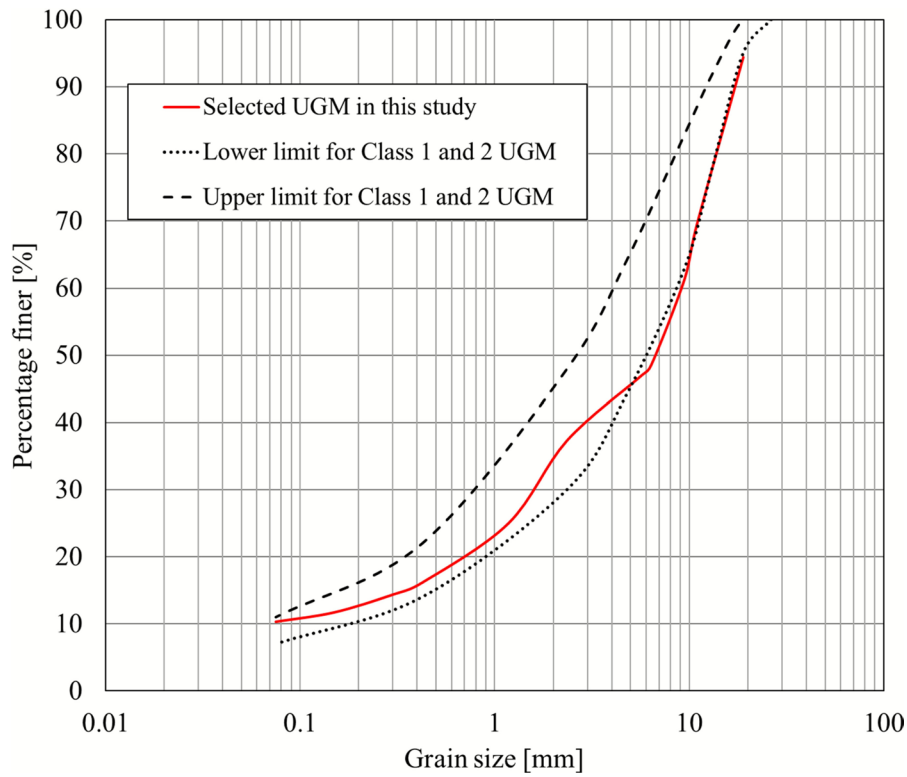

Fig. 1 Particle size distribution of selected unbound granular materials (Class 2). The upper and lower limits for Class 1 and 2 unbound granular materials are based on VicRoads guidelines (VicRoads 2017)

uniformity, two subsamples were collected immediately after mixing, and two additional subsamples were obtained after compaction to determine the initial moisture content using the oven-drying method. The prepared samples were then compacted separately in two wooden moulds, each measuring 250 mm × 125 mm × 150 mm, as illustrated in Fig. 2a–c. Wooden moulds were chosen for their compatibility with microwave drying, as metal moulds pose safety risks due to microwave reflection. The mould dimensions were determined based on numerical simulations using COMSOL Multiphysics®, ensuring effective heat dissipation within the compacted samples while reducing microwave

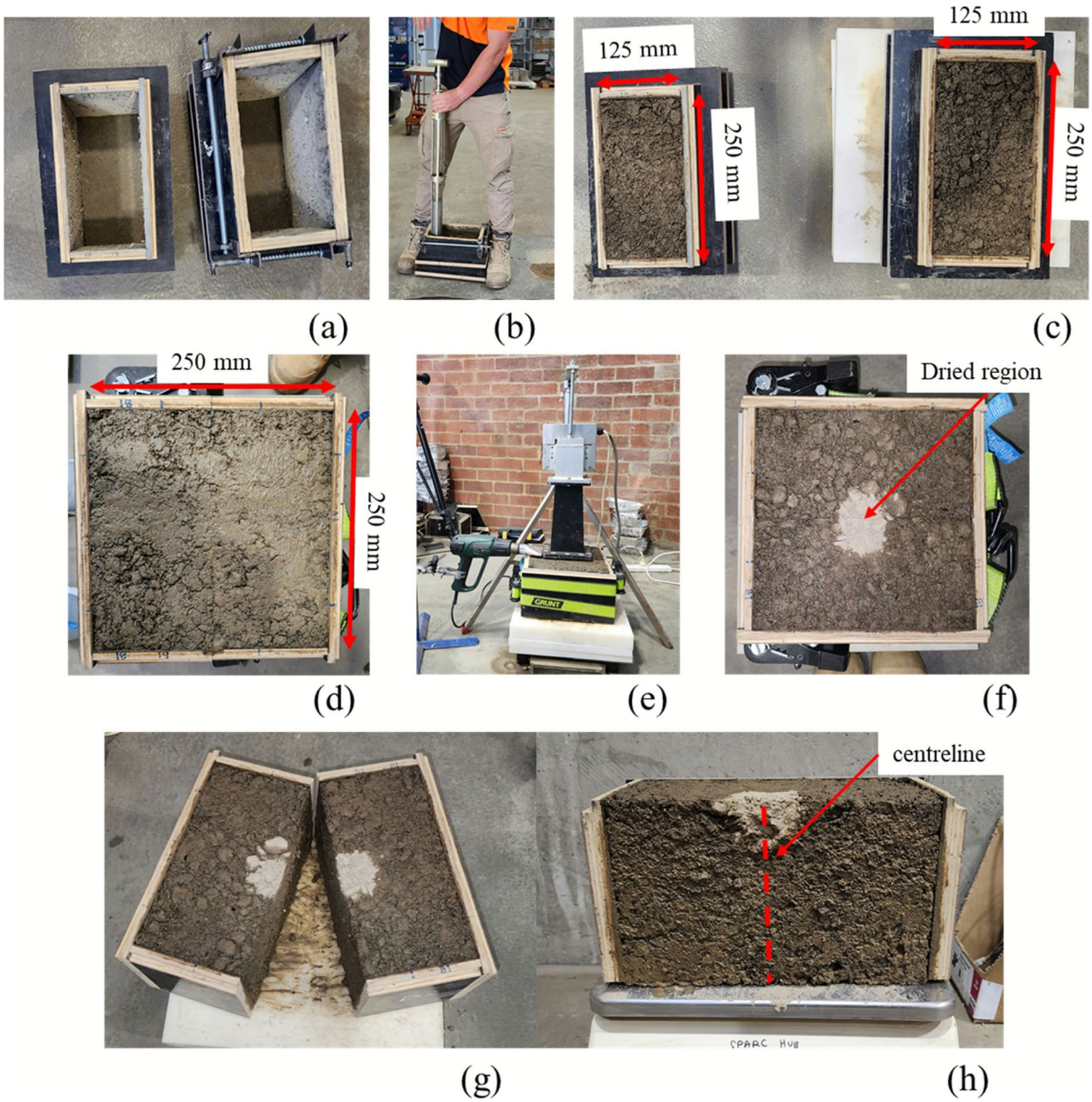

Fig. 2 Experimental stages: **a** two empty wooden moulds, **b** compaction of unbound granular materials, **c** compacted unbound granular materials in two wooden moulds, **d** combined UGM sample, **e** microwave convective drying of compacted UGM sample, **f** UGM sample after microwave convective drying, **g** split UGM sample for data collection, and **h** cross-sectional view of UGM sample after drying

interaction with the mould and minimising potential boundary effects on heat and moisture transfer during the drying process.

The use of two separate moulds enabled the assessment of temperature and moisture variations at the centre depth and allowed visual inspection of drying depth progression (Fig. 2g-h). Although this approach potentially introduces variability in drying behaviour, careful attention was paid to ensure minimal air gaps between the moulds, reducing potential heat loss or moisture escape. A rammer weighing 4.9 kg was used to compact the material in two layers within each mould, applying 300 drops per layer. After compaction, the two moulds were combined to form a single sample measuring 250 mm × 250 mm × 150 mm, as depicted in Fig. 2f. The prepared sample was then subjected to microwave convective drying, as shown in Fig. 2e. After drying, visual observation and measurements for moisture content and temperature were taken to evaluate the effectiveness of the drying process, as presented in Fig. 2f-h.

3.2 Experimental Equipment and Procedure

The UGM specimens were subjected to microwave convective drying using a small-scale microwave applicator combined with a heat gun (Bosch PHG 630DCE), as illustrated in Fig. 3a. The applicator consisted of an open-ended horn antenna with aperture dimensions of 110 mm × 55 mm, specifically designed to focus microwave energy onto the compacted UGM. The antenna was connected to a waveguide (86 mm × 43 mm), powered by a 900 W magnetron sourced from a commercial microwave oven operating at 2.45 GHz, as detailed in Fig. 3. To ensure a safe working environment, all experiments were conducted in an isolated area and periodic checks made using a microwave leakage detector (Extech 480,846) to confirm radiation levels remained below the allowable time-averaged exposure to electric fields of 137 V/m rms at 2.45 GHz (Australian Radiation Protection and Safety Agency 2002).

The heat gun featured three adjustable airflow speed settings and temperature settings from 50–630 °C. It was mounted on a tripod, enabling precise adjustments of the airflow angle. A 75 mm wide nozzle was attached to the heat gun to distribute airflow uniformly across the compacted UGM sample surface. Microwave convective drying experiments were conducted on compacted UGM samples by systematically varying four key parameters: air temperature, airflow speed, airflow angle, and drying duration. The selected test conditions for microwave convective drying experiments are summarised in

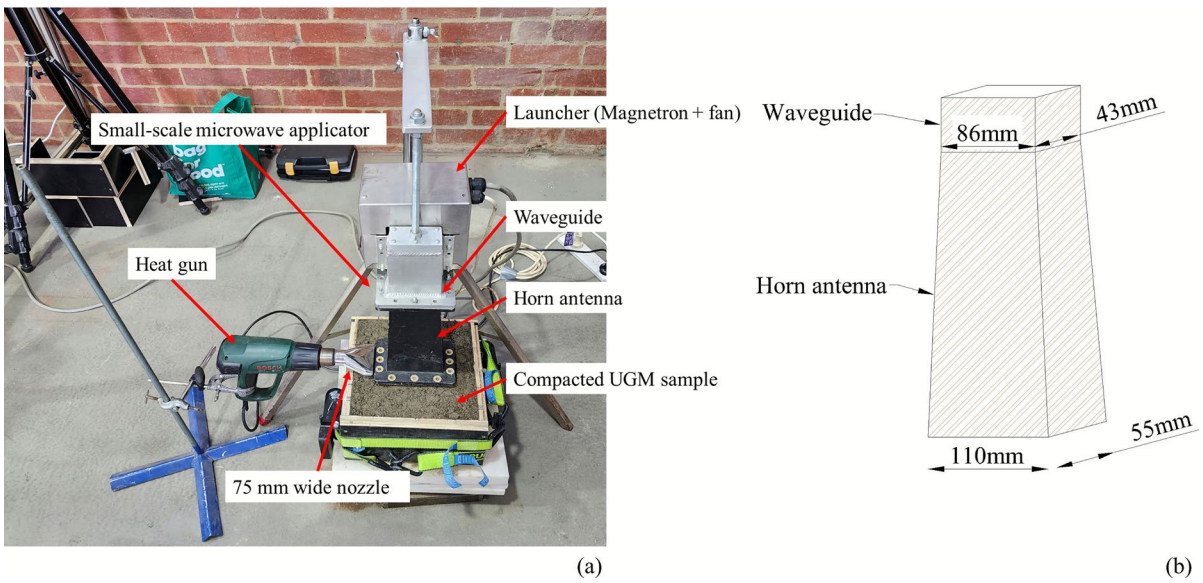

Fig. 3 **a** Experimental arrangement for microwave convective drying of a compacted UGM sample, and **b** schematic diagram of the horn antenna and waveguide with dimensions as shown

Table 2 Test conditions of the microwave convective drying of compacted unbound granular materials

Test	Air temperature [°C]	Airflow angle [°]	Speed level of the airflow (Speed of the airflow [m/s])	Drying time [minutes]
T1	120	18	Level II (3.6)	4
T2				6
T3		45	Level II (3.6)	4
T4				6
T5			Level III (4.3)	4
T6				6
T7	150	18	Level II (3.6)	4
T8				6
T9		45	Level II (3.6)	4
T10				6
T11			Level III (4.3)	4
T12				6

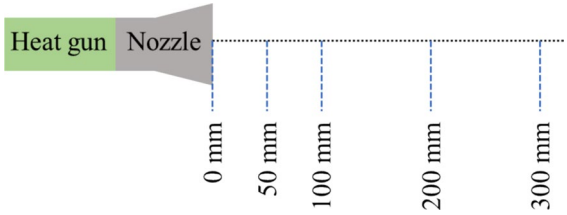

Fig. 4 Schematic illustration of the measurement points from the centre of the nozzle during the calibration process

Table 2. Given the labour-intensive nature of sample handling, including compaction and lifting, only two sets of parameters for each variable were explored during the laboratory investigation.

3.2.1 Heat Gun Calibration

The test conditions presented in Table 2 required careful calibration of the heat gun to achieve efficient drying and to maintain laboratory safety. Calibration involved measuring air temperature and airflow speed at varying distances from the nozzle centre (Fig. 4) using N-type thermocouples and a hand-held anemometer (Protech QM1647). Prior research by Athmarajah (2025) indicated that the surface temperature of the compacted UGM samples exceeded 100 °C during microwave drying. To enhance drying efficiency while ensuring safety, preliminary calibrations explored optimal hot air temperatures of around 100 °C.

Initial calibration, as shown in Fig. 5, demonstrated a significant drop in airflow temperature with distance from the nozzle. These measurements were conducted in open air without any sample placed in front of the nozzle or any obstruction in the surrounding testing area, allowing for characterisation of the natural decay of airflow temperature with distance. Based on these results a temperature setting of 150 °C was selected to achieve a target surface temperature

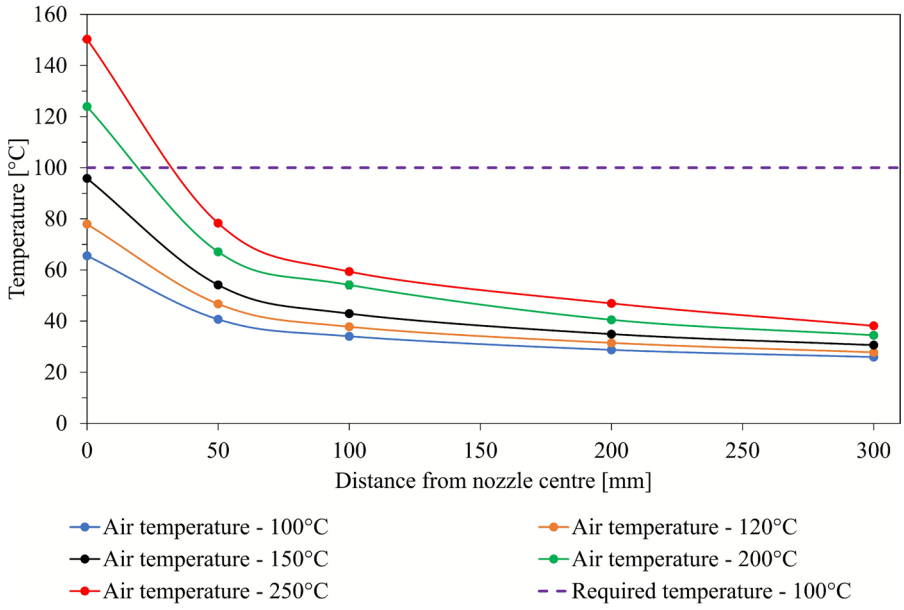

Fig. 5 Variation in air temperature with the distance from the centre of the attached nozzle

of approximately 100 °C during microwave convective drying. Although initial results (Fig. 5) suggested that 150 °C would be optimal, a slightly lower temperature of 120 °C was adopted for comparative experiments to prioritise safety considerations in the laboratory.

It should be noted that the heat gun's lowest airflow setting (level I) provided airflow at a fixed temperature of approximately 50 °C, which was insufficient for the intended drying experiments. Therefore, only speed levels II and III, which offered adjustable temperatures ranging from 50–630 °C, were utilised in this study. As the hot air temperature dropped with distance from the centre of the nozzle, as depicted in Fig. 5, the heat gun nozzle was positioned at the edge of the microwave horn antenna (approximately 60 mm away from the aperture centre) during the laboratory experiments, as shown in Fig. 6, to ensure consistent drying processes. Further, speed measurements were taken near the nozzle and at a distance of 50 mm from the nozzle's centre using a hand-held anemometer. For speed level II, the measured speed values were 3.6 m/s near the nozzle and 2.8 m/s at a 50 mm distance. Similarly, for speed level III, the measured speed values were 4.3 m/s near the nozzle and 3.4 m/s at a 50 mm distance.

3.2.2 Microwave Convective Drying Process

All of the test conditions were conducted with a consistent gap of 10 mm between the antenna aperture and the compacted UGM surface. Figure 6 shows the arrangements of the heat gun for different angles of the airflow. Due to the design of the nozzle, maintaining a parallel airflow angle to the surface of the compacted UGM sample posed a challenge in aligning the airflow with the gap between the antenna and the material surface. Consequently, adjustments were made to the angle of airflow (~ 18°) to align the nozzle opening with the gap between the antenna and the material surface (Fig. 6a). Before each experiment, the angle with respect to the ground or surface of the UGM sample was carefully measured using a digital inclinometer, ensuring consistency in the test conditions.

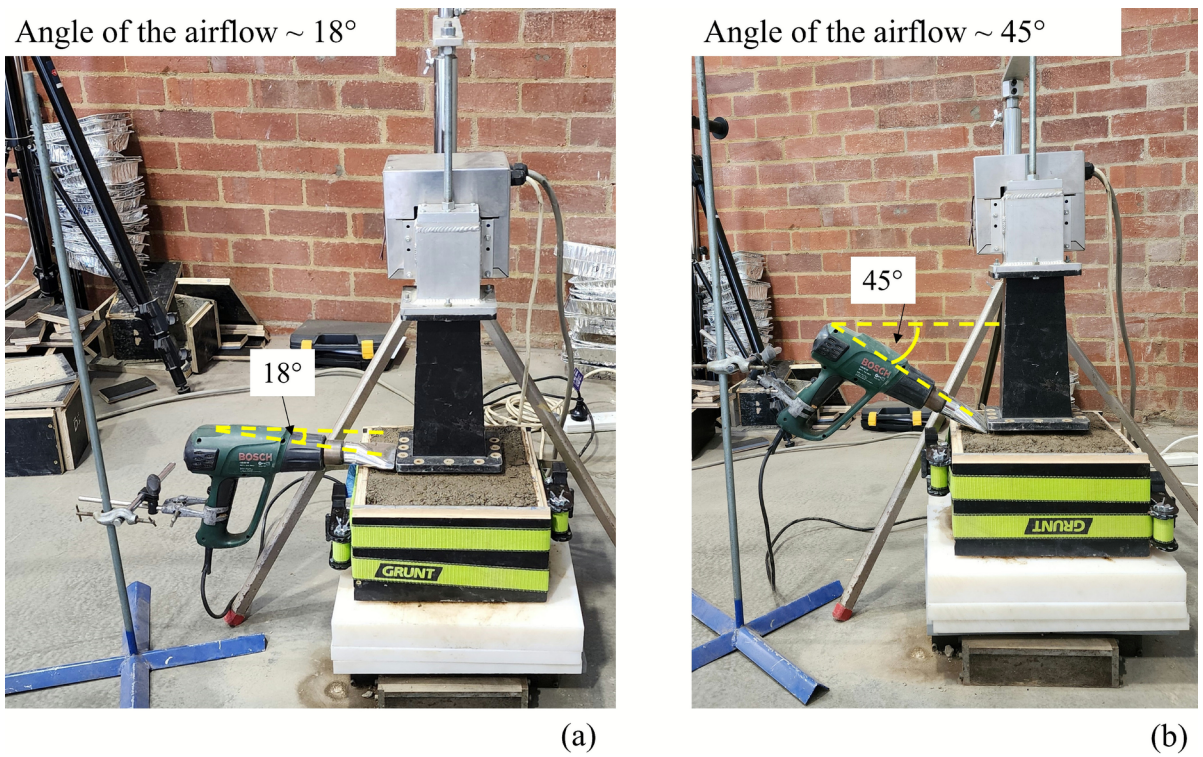

Fig. 6 Arrangements of the heat gun for different angles of the airflow: **a** Angle of the airflow ~ 18°, and **b** Angle of the airflow ~ 45°

After each drying process, surface temperature variations were recorded using an infrared (IR) thermal imaging camera (FLIR B200). Thermal images were captured immediately after microwave convective drying to minimise the samples' exposure to environmental conditions. The thermal imaging camera was professionally calibrated prior to testing to verify the accuracy (±2 ℃) (FLIR Systems 2009). Following the thermal imaging, the combined sample was separated, and the post-drying moisture distribution was assessed by core sampling along the centreline of the specimen (Fig. 2h). Approximately 20 mm × 40 mm core samples were extracted at 50 mm intervals along the depth from the surface of the compacted UGM sample. Due to the limited volume of the visibly dried zone, one core sample was collected at each depth for gravimetric moisture determination.

The degree of saturation (S_r) at each depth was calculated based on the measured gravimetric water content, the known specific gravity of solids, and the dry density. The dry density was assumed to remain constant throughout the drying process due to the low fine content of the material and its minimal shrink-swell potential. While special care was taken during sample preparation and testing, potential sources of error include slight moisture loss during handling and coring processes. A summary of initial conditions, including moisture content, dry density and initial S_r for each test condition, is provided in Table 3.

The microwave convective drying process resulted in a visible dried region on the surface of the compacted UGM (Fig. 2f), exhibiting an approximately elliptical shape as illustrated in Fig. 7a. Similarly, the dried region over the depth (Fig. 2h) exhibited a semi-elliptical profile along the centreline of the compacted UGM, as shown in Fig. 7b. The area of the dried region on the surface (A) and total dried volume (V) were calculated based on three main measurements: the major axis length (a), the minor axis length (b), and the drying depth (h).

3.3 Machine Learning Model Development

This study explored the use of machine learning models to predict the drying behaviour of an UGM subjected to microwave convective drying. Due to the labour-intensive and time-consuming nature of laboratory experiments, the number of experimental tests was limited, resulting in a relatively small dataset. Therefore, machine learning models were employed to efficiently analyse the available data, identify the critical parameters influencing the drying performance, and provide insights into the drying behaviour within and near the tested experimental conditions.

The dataset for the machine learning models was derived from experimental results that included six features: initial S_r, air temperature, airspeed, airflow angle, drying time, and depth from the

Table 3 Initial conditions of compacted UGM samples used in microwave convective dry-back experiments

Test	Initial gravimetric moisture content ± 1standard deviation [(w/w), %]	Dry density [kg/m^3]	Initial degree of saturation, $S_{r,\text{initial}}$ [%]
T1	5.6 ± 0.3	2379.6	91.9
T2	5.9 ± 0.1	2359.6	91.8
T3	5.9 ± 0.4	2359.9	91.7
T4	5.8 ± 0.3	2372.2	93.4
T5	5.8 ± 0.4	2363.2	91.3
T6	5.9 ± 0.3	2358.9	91.6
T7	5.1 ± 0.2	2383.6	85.6
T8	5.1 ± 0.3	2396.4	88.4
T9	5.8 ± 0.4	2362.8	91.2
T10	5.9 ± 0.3	2361.1	92.2
T11	5.9 ± 0.3	2364.7	92.8
T12	5.9 ± 0.3	2365.2	92.9

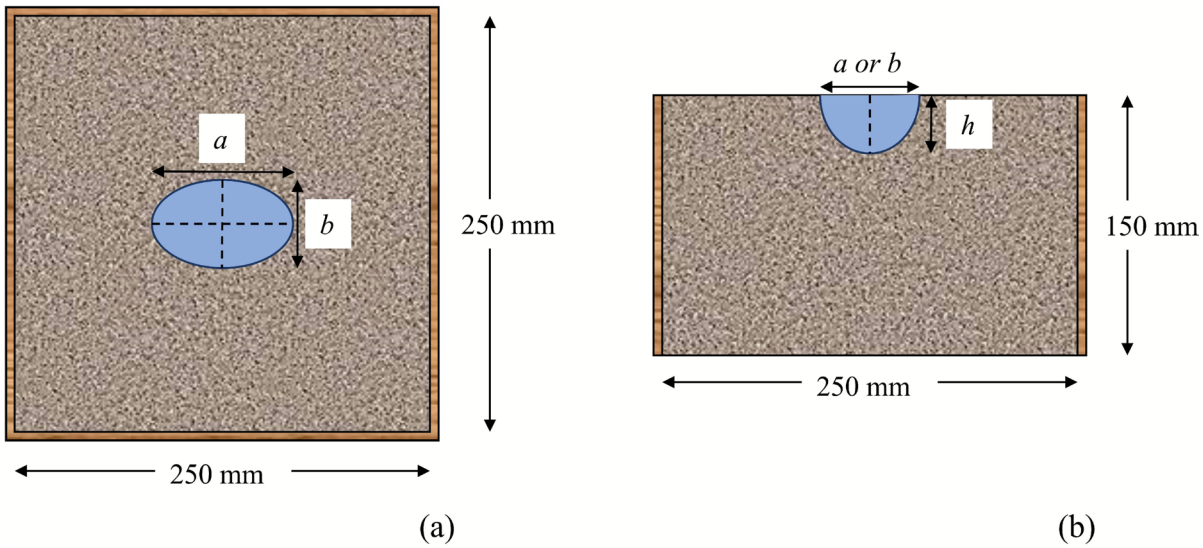

Fig. 7 Schematic representation of dried region after microwave convective drying: **a** on the surface and **b** over the depth of the compacted UGM sample

material surface. As all experiments were conducted at constant microwave power, this parameter was not included in the analysis. Additionally, since a single UGM type with consistent gradation and material-specific properties (e.g., specific gravity and Atterberg limits) was used across all tests, separate material parameters were not included as model inputs. The target variable was the ratio between the final degree of saturation ($S_{r,final}$) and the initial degree of saturation ($S_{r,initial}$) defined as

$$S_r ratio = \frac{S_{r,\text{final}}}{S_{r,\text{initial}}} \times 100 \tag{7}$$

The S_r ratio represents a normalised indicator of drying efficiency, allowing for meaningful comparisons across varying initial saturation levels. Since initial S_r is already included as an input, using the S_r ratio as the model output ensures consistency while preserving the impact of the starting moisture condition. The dataset consists of 84 data points, with the minimum, maximum, and mean values of each input parameter summarised in Table 4.

The SVM and GPR models were selected for this study due to their better handling of small datasets (Mountrakis et al. 2011). Data pre-processing steps included normalisation and splitting of the dataset into training (80%) and testing (20%) sets. To minimise the risk of overfitting associated with the limited dataset size (n = 84), a five-fold cross-validation procedure was applied during model training. Performance metrics such as coefficient of determination (R^2) and mean absolute error (*MAE*) were used to evaluate the robustness of the models.

Table 4 Summary of input parameters used for machine learning models

Input parameter	Number of data points	Mean	Minimum	Maximum
Initial S_r (%)	84	89.3	85.1	93.4
Air temperature (°C)	84	75	0	150
Airflow angle (°)	84	22.5	0	45
Airspeed (m/s)	84	2.2	0	4.3
Drying time (minutes)	84	3	0	6
Depth (mm)	84	75	25	125

4 Results and discussion

4.1 Machine Learning Model Results

Figure 8 illustrates the comparison between the actual S_r ratio and the predicted values obtained from the

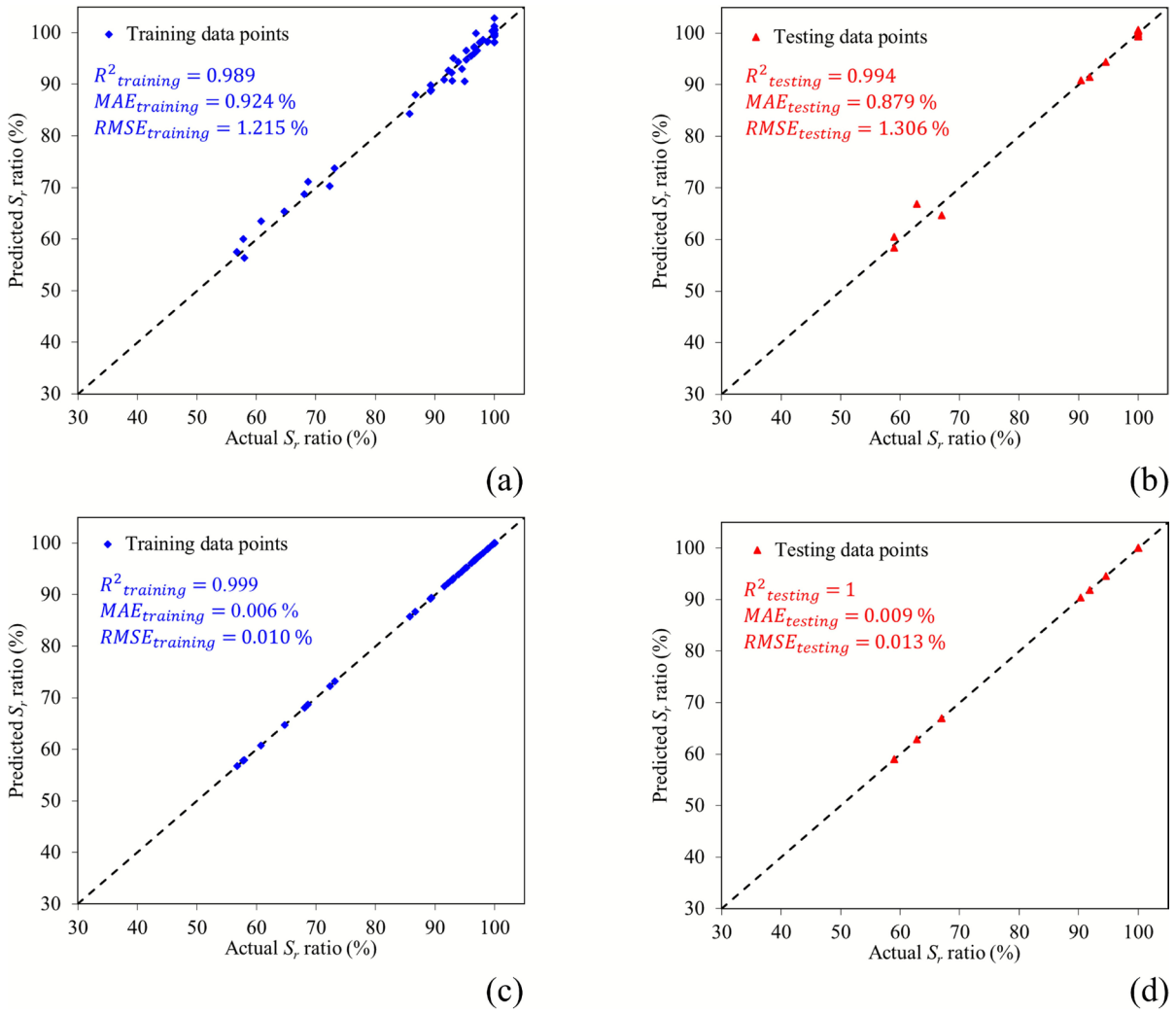

Fig. 8 Comparison between actual S_r ratio and predicted S_r ratio: **a** SVM training dataset, **b** SVM testing dataset, **c** GPR training dataset, and (d) GPR testing dataset (MAE – mean absolute error, RMSE – root mean square error)

SVM and GPR models. Both models effectively captured the drying trends, with GPR showing slightly better prediction accuracy. The optimal parameters obtained after training the SVM and GPR models are given in Table 5. In machine learning, model parameters refer to values learned directly from the training data (such as weights or coefficients), whereas hyperparameters are predefined values that control the learning process. Examples of hyperparameters include the kernel function, box constraint, and epsilon in SVM, or the length scale in GPR. These are typically selected through a tuning process to optimise model performance before the model training.

Although the selected models demonstrated high predictive accuracy, their use in this study also provided a structured framework to assess variable sensitivities and interactions across different depths, complementing the experimental findings. However, the models can only be reliably applied within the specific conditions represented in the dataset. All tests were conducted on a single UGM type compacted under similar conditions and dried using a fixed microwave power. In addition, the trained SVM and GPR models are valid only within the ranges of air temperature, airflow speed, airflow angle, drying time, and depth represented in the

Table 5 Optimal hyperparameters found for the selected Support Vector Machine (SVM) and Gaussian Process Regression (GPR) machine learning models after training

Machine learning model	Hyperparameter	Value	Description
SVM	Epsilon	0.5899	Insensitive margin within which no penalty is given for training error
	Kernel function	Polynomial	Defines the transformation applied to input data
	Kernel polynomial order	3	Degree of the polynomial kernel
	Kernel scale	1.85	Affects the width of the decision boundary in the transformed space
	Box Constraint	5.89	Controls trade-off between smoothness and training error
GPR	Kernel function	Matern52	Defines the covariance structure of the model
	Length scale	2.7378	Controls the smoothness of the function being estimated
	Standard deviation	0.1298	Influences the vertical scale (range) of predicted values

dataset (Table 4), and extrapolation beyond these ranges or to different materials, compaction states, or microwave configurations is limited. Therefore, future work is recommended to broaden the applicability of these models by incorporating larger and more diverse datasets.

To evaluate the predictive capability of the developed machine learning models, the predicted S_r trends from both the SVM and GPR models were plotted alongside the experimental results for selected test conditions. These overlays allow direct comparison of predicted and observed trends at specific experimental combinations. This approach enables validation of the models within the tested range while providing a clear visual comparison of model accuracy.

4.2 Effect of Temperature of Hot Airflow

The effect of hot air temperature on the efficiency of microwave convective drying was investigated under controlled conditions, maintaining a consistent airflow angle of about 45° and speed level II. Four sets of test conditions denoted as T3, T4, T9 and T10, were compared to assess the impact of varying hot air temperatures (120 °C and 150 °C) for drying durations of 4 and 6 min. Figure 9 shows the variations in S_r at the centre of the compacted UGM sample (Fig. 9a), IR thermal images for different test conditions (Fig. 9b), and the calculated area and volume of the visible dried region in the compacted UGM sample after microwave convective drying (Fig. 9c).

Despite the variations in hot air temperature, the S_r variations at the centre of the compacted UGM sample did not exhibit noticeable differences for either drying duration, as can be seen in Fig. 9a. This observation suggests that, within the specified experimental parameters, alterations in hot air temperature did not profoundly influence the moisture removal at the core of the compacted UGM samples. Further examination of IR thermal images showed that after 4 min of drying, the maximum surface temperature reached 102 ℃ for an air temperature of 120 ℃ and 104 ℃ for an air temperature of 150 ℃. After 6 min of drying the maximum surface temperatures were 119 °C for 120 °C air temperature and 118 °C for 150 °C air temperature. These results indicate that the maximum surface temperature after microwave convective drying was nearly identical for both air temperatures. However, the dried area at the surface expanded from 81.85 cm^2 at 120 °C to 97.77 cm^2 at 150 °C after 4 min of drying. Similarly, after 6 min of drying, a visible increase in the dried area at the surface was observed with higher hot air temperatures (i.e., from 81.85 cm^2 at 120 °C to 119.95 cm^2 at 150 °C). This phenomenon indicated that higher air temperatures facilitated a wider drying spread at the surface of the compacted UGM layer.

Contrary to surface observations, analysis of cross-sectional images (Fig. 9c) revealed that the depth of visible drying remained around 24 mm—28 mm after 4 min of drying and 32 mm—37 mm after 6 min of drying for both air temperatures, indicating that increasing air temperatures had no substantial impact on the dried depth within the compacted UGM samples. This discrepancy between the surface and depth indicates that while higher hot air temperatures may enhance surface drying, they do not necessarily correspond to deeper moisture removal

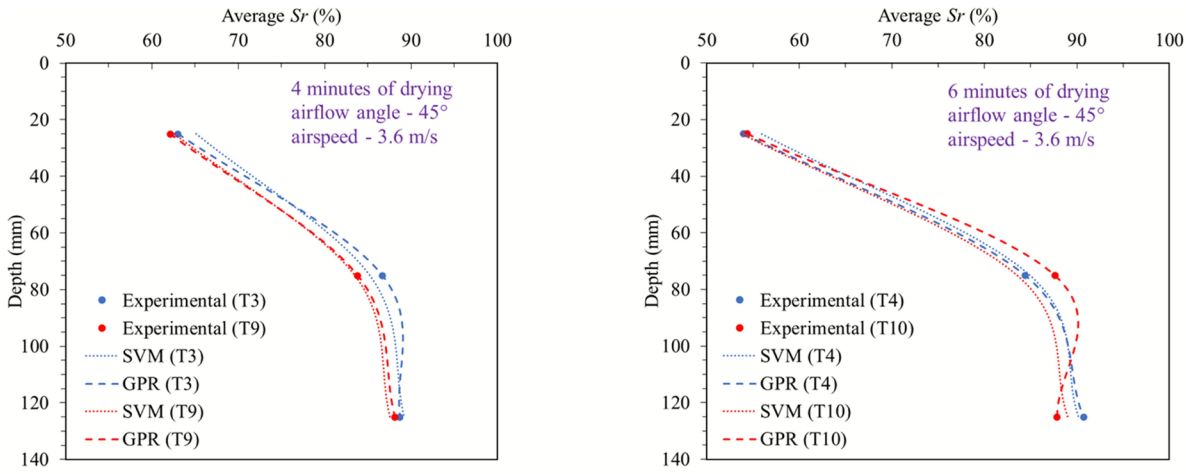

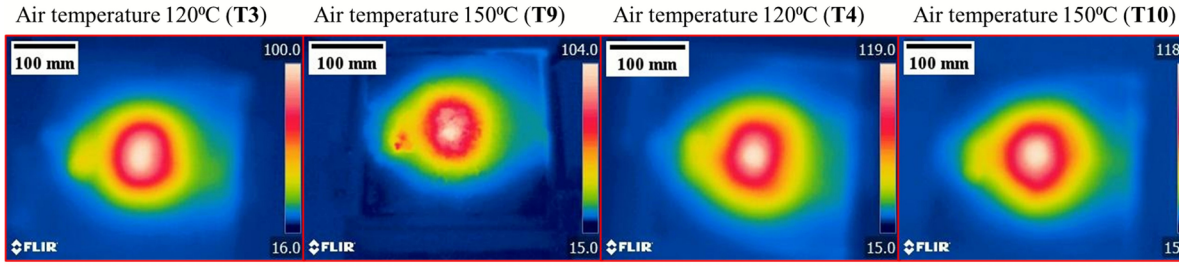

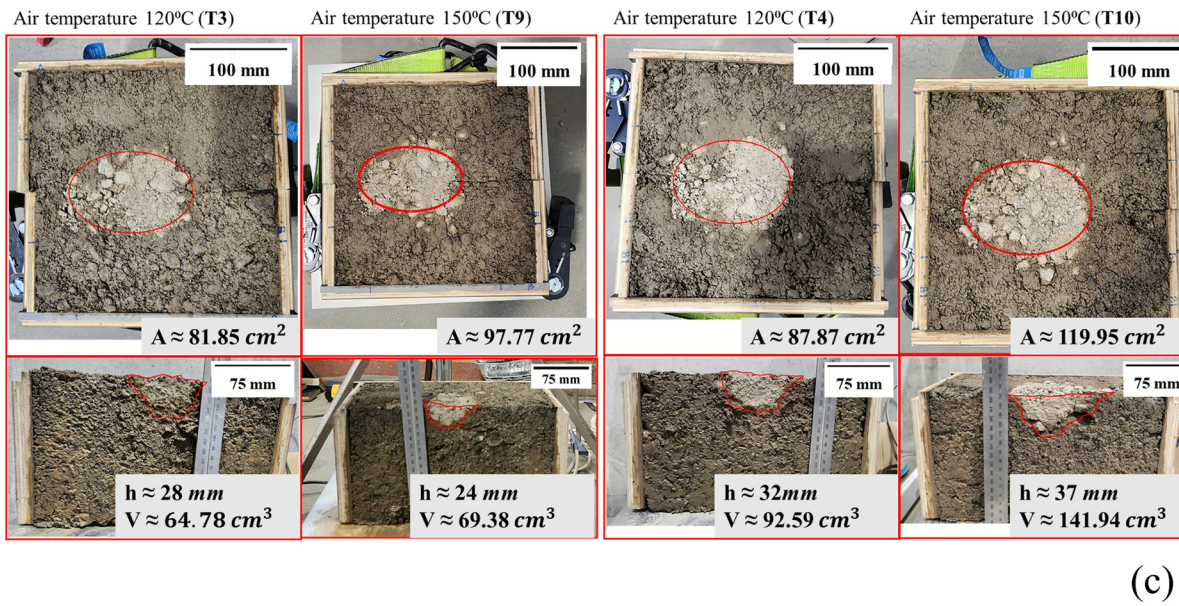

Fig. 9 Comparison of the effect of air temperature on the drying efficiency of test conditions T3, T4, T9 and T10: **a** Variation in S_r at the centre, **b** IR thermal images, and **c** Comparison of area and volume of the dried region after microwave convective drying process of compacted UGM samples (T3 and T4 represent air temperature 120 ℃, while T9 and T10 correspond to air temperature of 150 ℃)

within the compacted UGM samples. However, it is noteworthy that despite the limited drying depth, the increased dried area at the surface resulted in a higher overall dried volume of the sample for higher hot air temperatures.

4.3 Effect of Angle of Hot Airflow

The impact of the airflow angle on the efficiency of microwave convective drying of compacted UGM samples was also explored. The study comprised two sets of drying durations (4 and 6 min) conducted at two distinct angles of airflow: 18° (T1 and T2) and 45° (T3 and T4), all carried out at a constant hot air temperature of 120 °C and speed level III, as shown in Fig. 10.

Analysis of the S_r at the centre of the compacted UGM samples revealed notable differences based on the angle of the airflow, as shown in Fig. 10a. Specifically, an increase in the airflow angle from 18° to 45° led to noticeable variations in S_r near the surface of the compacted UGM samples, indicating enhanced drying in the surface layers. Further examination of IR thermal imaging indicated that for 4 min of drying, the maximum surface temperature remained nearly identical at 102 °C for an 18° airflow angle and 100 °C for a 45° airflow angle. However, with an extended drying duration of 6 min, the maximum surface temperature increased to 108 °C at an 18° airflow angle and 119 °C at a 45° airflow angle. This result suggests that increasing the airflow angle may enhance the heat distribution at the surface, but only over extended drying periods.

Visual inspection of the plan and sectional images of dried UGM samples (Fig. 10c), along with the calculated area and volume measurements for the visible dried region in the compacted UGM sample after drying, supports the findings. After 4 min of drying, increasing the airflow angle from 18° to 45° led to an expansion of the dried area at the surface from 34.10 cm^2 to 81.85 cm^2. Likewise, after 6 min, the dried area grew from 68.19 cm^2 at 18° to 87.87 cm^2 at 45°, demonstrating more pronounced drying of the surface at a higher airflow angle. Despite these improvements in surface drying, there was no significant enhancement in the depth of the visible dried region, as shown in Fig. 10c, suggesting that changes in airflow angle primarily influenced only the drying near the surface of the compacted UGM sample.

Overall, the experimental investigation indicated that a higher airflow angle facilitated more efficient removal of moisture near the surface of the compacted UGM samples, particularly over extended drying durations. However, it is important to note that while changes in the airflow angle benefit surface drying, they did not significantly impact the depth of the visible dried region. These findings emphasise the potential of higher airflow angles during microwave convective drying for enhancing surface drying in the compacted UGM layer, which could have beneficial implications for pavement dry-back processes.

4.4 Effect of Speed of Hot Airflow

The influence of the speed of the hot airflow on the efficiency of microwave convective drying was investigated by keeping a constant hot air temperature of 150 °C and an angle of airflow of 45°. The test conditions considered in this analysis were T9 and T10 at airflow speed level II (3.6 m/s) with drying times of 4 and 6 min, and T11 and T12 at airflow speed level III (4.3 m/s) with drying times of 4 and 6 min. As discussed in the previous section, a higher airflow angle led to enhanced drying near the surface of the compacted UGM sample. Therefore, the effect of speed level III was explored at the airflow angle of 45° to minimise labour-intensive work during the laboratory experiments. Variations in S_r along the depth of the compacted UGM sample, IR thermal images and the area and volume of the dried region after microwave convective drying are presented in Fig. 11.

After 4 min of microwave convective drying, an increase in the airflow speed from 3.6 m/s (Level II) to 4.3 m/s (Level III) resulted in enhanced drying near the surface of the sample, as evidenced by the variations in S_r along the depth of the compacted UGM samples (Fig. 11a). This result can be attributed to the higher airflow speed facilitating more efficient moisture removal from the surface layers of the sample. However, no significant differences were observed in S_r along the centre of the sample after 6 min of drying for both airflow speeds, suggesting a potential equilibrium state in moisture removal. Moreover, it should be noted that other factors: initial S_r and density of the compacted UGM samples may also have affected the efficiency of the microwave convective drying of the compacted UGM samples.

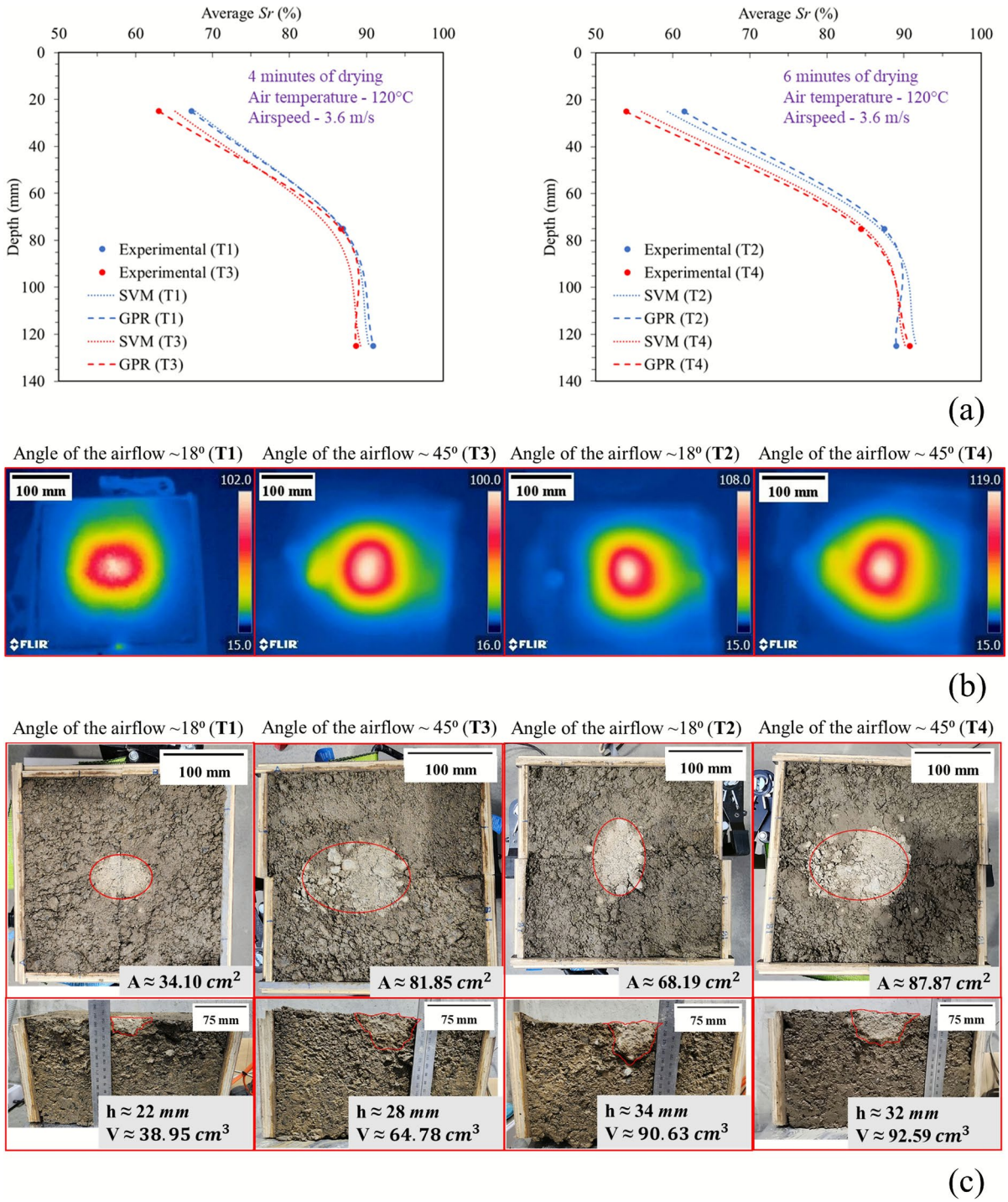

Fig. 10 Comparison of the effect of airflow angle on the drying efficiency of test conditions T1, T2, T3 and T4: **a** Variation in S_r at the centre, **b** IR thermal images, and **c** Comparison of area and volume of the dried region after microwave convective drying process of compacted UGM samples (T1 and T2 represent an airflow angle of 18°, while T3 and T4 correspond to the airflow angle of 45°)

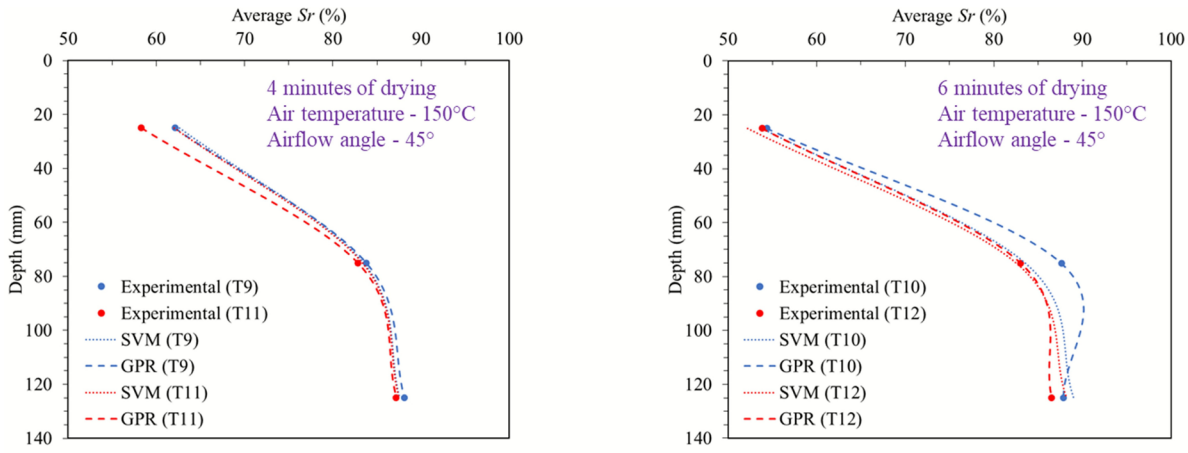

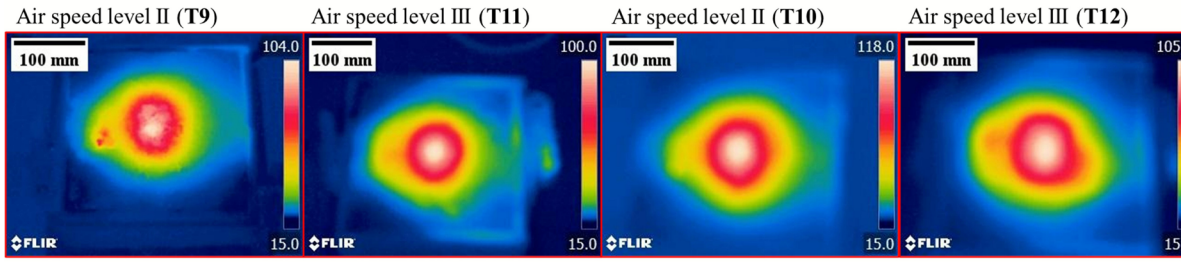

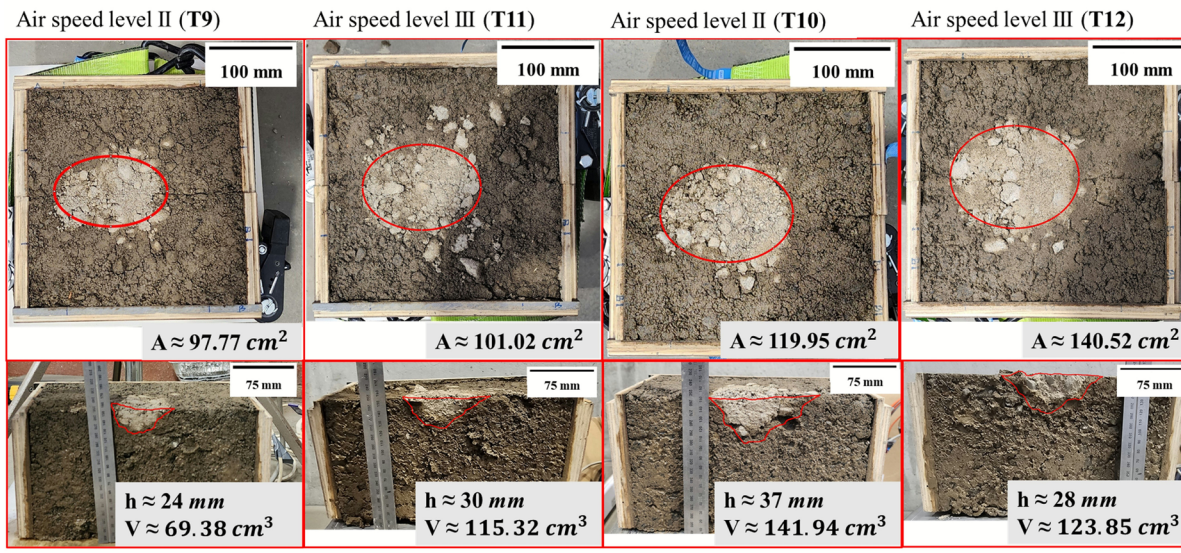

Fig. 11 Comparison of the effect of airflow speed on the drying efficiency of test conditions T9, T10, T11 and T12: **a** Variation in S_r at the centre, **b** IR thermal images, and **c** Comparison of area and volume of the dried region after microwave convective drying process of compacted UGM samples (T9 and T10 represent airspeed level II of 3.6 m/s, while T11 and T12 correspond to airspeed level III of 4.3 m/s)

Interestingly, IR thermal images shown in Fig. 11b presented another dimension to this phenomenon. After 4 min of drying, the maximum surface temperature was 104 ℃ at speed level II and 100 ℃ at speed level III, being slightly lower at the higher airflow speed. A similar drying trend was observed after 6 min of drying, with maximum surface temperatures of 118 ℃ for speed level II and 105 ℃ for speed level III. This observation could be explained by the increased speed of airflow, enhancing the removal of moisture near the surface, resulting in higher evaporative cooling near the surface of the material and reducing the surface temperature of the compacted UGM sample (Tuffour et al. 2014).

While increasing the airflow speed resulted in a larger visible area of the dried region, as shown in Fig. 11c, indicating improved surface drying, there was no substantial impact on the depth of the visible dried region within the sample. Despite this, the increased area of the dried region and slight variations in depth contributed to an overall increased volume of the dried region with the increasing airspeed. However, although the area of the dried region increased for higher airflow speeds for 6 min of drying, the depth of the dried region was reduced compared to lower airflow speeds, resulting in a lower volume of the dried region. This discrepancy could be attributed to potential errors during the laboratory experiments, such as the manual positioning of the microwave applicator and heat gun and differences in initial material conditions of the UGM such as S_r and density.

In summary, increasing airflow speed may benefit the dry-back process in road construction by promoting enhanced surface drying of compacted granular layers while concurrently reducing surface temperatures. However, it is important to note that while higher airflow speeds improved surface drying efficiency, they did not substantially impact the depth of drying within the sample.

4.5 Effect of Drying Time

The effect of drying time on the drying efficiency of microwave convective drying of compacted UGM samples was studied by maintaining a constant air temperature of 150 °C and speed level II. The study included two sets of drying durations (4 and 6 min) conducted at two distinct angles of airflow: 18° (T7 and T8) and 45° (T9 and T10).

As illustrated in Fig. 12a, extending the duration of microwave convective drying resulted in noticeable enhancements in drying efficiency, particularly at the surface of the samples, for both angles of the airflow. This observation is aligned with expectations, as increased drying time allows for more moisture removal from the material. However, it is essential to note that test conditions T7 and T8 exhibited lower initial moisture contents than T9 and T10, resulting in a lower final S_r at the centre after the drying. The thermal images depicted in Fig. 12b illustrate an increase in the maximum surface temperature of the compacted UGM samples with longer drying durations. Moreover, analysis of plan and sectional images yielded that the area of the visible dried region increased proportionally with drying time, indicating improved surface drying. After 4 min of drying, the dried area measured 97.88 cm^2 at 18° and 97.77 cm^2 at 45°, but with an extended drying time of 6 min, it expanded to 118.96 cm^2 and 119.95 cm^2, respectively. Notably, the depth of the dried region also increased as depicted in Fig. 12c, ranging from 24 to 30 mm after 4 min to 37 mm after 6 min, demonstrating that longer drying durations contribute to improved moisture extraction not just at the surface, but to some extent, at greater depths as well.

While the previous sections observed that factors including air temperature, angle and airflow speed did not enhance the drying at the core of the compacted UGM samples at different drying durations, further comparative analysis between the efficiency of microwave drying and microwave convective drying of UGM at different durations is required to understand the drying dynamics across varying drying conditions.

4.6 Comparative Analysis of the Efficiency of Microwave-only and Microwave Convective Drying

This comparative analysis explored the efficiency of microwave-only and microwave convective drying of compacted UGM samples for 4- and 6-min durations. For the reference microwave drying tests, a similar procedure was followed, but only the small-scale microwave applicator was used without the heat gun. In contrast, for the microwave convective drying

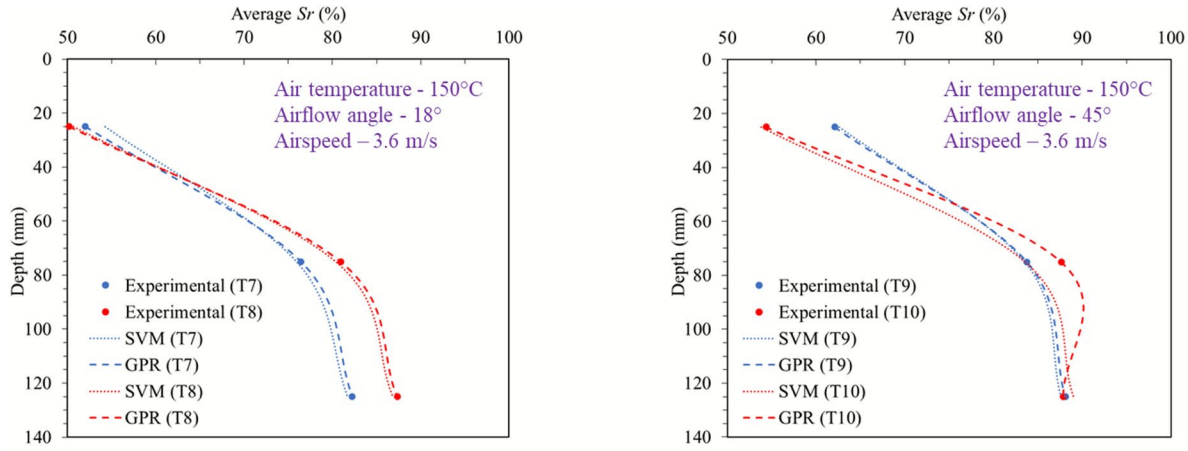
Average Sr (%)
50 60 70 80 90 100
0 20 40 60 80 100 120 140
Depth (mm)
Air temperature - 150°C
Airflow angle - 18°
Airspeed – 3.6 m/s
Experimental (T7)
Experimental (T8)
SVM (T7)
GPR (T7)
SVM (T8)
GPR (T8)
Average Sr (%)
50 60 70 80 90 100
0 20 40 60 80 100 120 140
Depth (mm)
Air temperature - 150°C
Airflow angle - 45°
Airspeed – 3.6 m/s
Experimental (T9)
Experimental (T10)
SVM (T9)
GPR (T9)
SVM (T10)
GPR (T10)

(a)

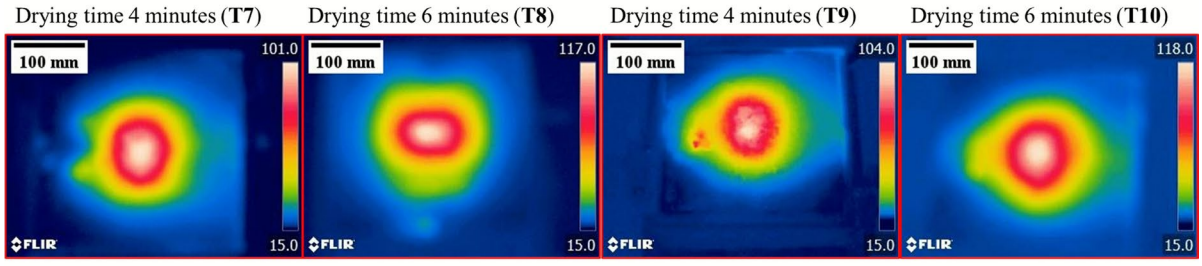
Drying time 4 minutes (T7)
Drying time 6 minutes (T8)
Drying time 4 minutes (T9)
Drying time 6 minutes (T10)
100 mm
101.0
117.0
104.0
118.0
15.0
FLIR

(b)

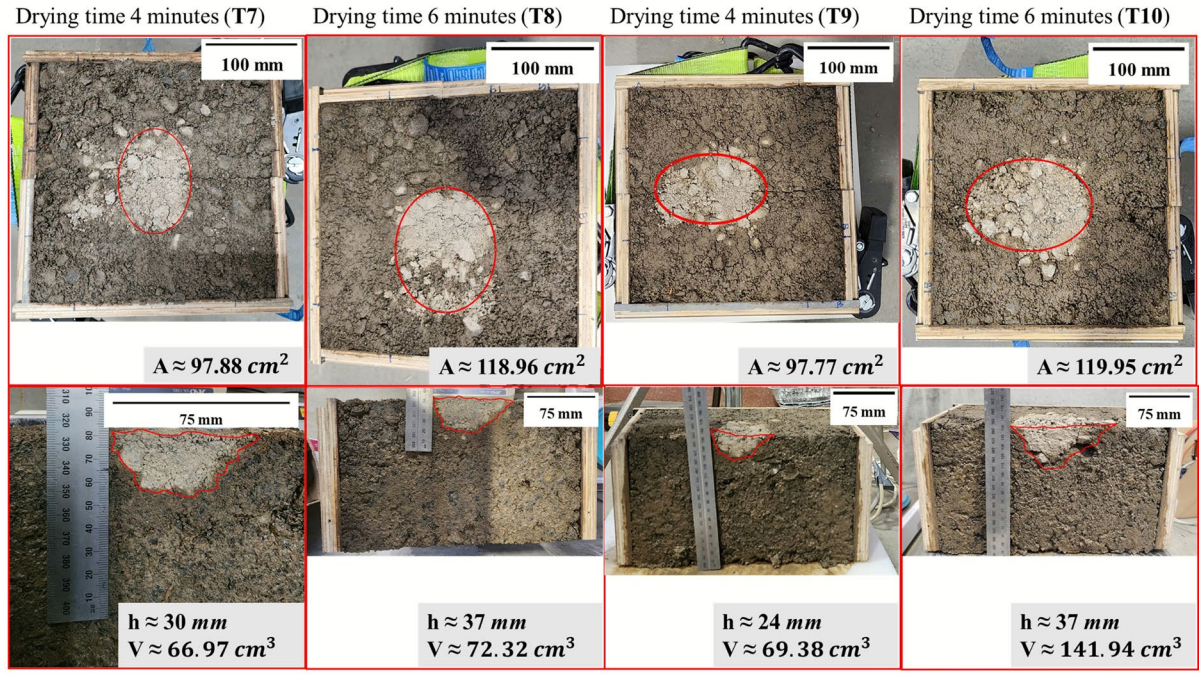
Drying time 4 minutes (T7)
Drying time 6 minutes (T8)
Drying time 4 minutes (T9)
Drying time 6 minutes (T10)
100 mm
75 mm
A ≈ 97.88 cm²
A ≈ 118.96 cm²
A ≈ 97.77 cm²
A ≈ 119.95 cm²
h ≈ 30 mm
V ≈ 66.97 cm³
h ≈ 37 mm
V ≈ 72.32 cm³
h ≈ 24 mm
V ≈ 69.38 cm³
h ≈ 37 mm
V ≈ 141.94 cm³

(c)

◂**Fig. 12** Comparison of the effect of drying duration on the drying efficiency of test conditions T7, T8, T9 and T10: **a** Variation in S_r at the centre, **b** IR thermal images, and **c** Comparison of area and volume of the dried region after microwave convective drying process of compacted UGM samples (T7 and T9 represent a drying duration of 4 min, while T8 and T10 correspond to 6 min)

analysis, test conditions such as T3 (air temperature 120 °C and speed level II), T5 (air temperature 120 °C and speed level III), T9 (air temperature 150 °C and speed level II), and T11 (air temperature 150 °C and speed level III) were selected over a 4-min duration (Fig. 13). For the 6-min drying duration, test conditions such as T4 (air temperature 120 °C and speed level II), T6 (air temperature 120 °C and speed level III), T10 (air temperature 150 °C and speed level II), and T12 (air temperature 150 °C and speed level III) were chosen for the comparative analysis (Fig. 14). All tests conducted at an airflow angle of 45° were considered for both drying durations.

Across both drying durations, the IR thermal images (Fig. 13a and Fig. 14a) show that the maximum surface temperatures were generally similar between the two drying methods. However, a noticeably wider temperature distribution was observed under microwave convective drying, indicating that the addition of hot airflow promoted a greater heat distribution across the sample surface. This broader region of elevated surface temperature distribution reflects the combined effect of volumetric microwave heating and the influence of forced convection, which can enhance heat transfer at the surface.

The surface images (Fig. 13b and Fig. 14b) consistently show that microwave convective drying produced a larger visibly dried region compared with microwave-only drying for both drying durations. This confirms that the convective component enhanced surface evaporation and increased the lateral spread of drying. However, the sectional images (Fig. 13c and Fig. 14c) reveal that the depth of visible drying remained almost identical between the two approaches. For both 4-min and 6-min tests, the depth of the dried region was confined to approximately 20—37 mm, indicating that the improved surface drying efficiency achieved through hot airflow did not translate into deeper moisture removal within the compacted UGM layer. Extending the drying duration from 4 to 6 min increased the dried area and dried volume under both drying methods, but did not meaningfully increase drying depth.

Overall, the comparative analysis confirmed that microwave convective drying enhanced surface moisture removal more effectively than microwave drying alone, as evidenced by the larger dried area and wider temperature distribution at the surface. Nevertheless, both methods exhibited similar limitations in drying depth, leading to non-uniform moisture distribution within compacted UGM samples—a challenge also observed in current solar dry-back practices (Athmarajah et al. 2023). Despite this limitation, microwave drying techniques demonstrated substantially faster drying rates than solar drying, making them a promising alternative for accelerating near-surface moisture removal in compacted granular pavement layers. While the solar dry-back process typically takes 3—4 days during summer conditions to achieve the required moisture levels (60% of S_r) in compacted UGM layers, and can extend up to 10 days under winter conditions, the microwave-based drying methods investigated in this and previous studies achieved comparable near-surface moisture reduction within 4—6 min (Athmarajah 2025).

To further assess the feasibility of microwave convective drying, a comparative energy analysis was conducted for the near-surface zone (0–50 mm), where both solar and microwave-based methods exhibited the highest moisture removal. The methodology, climatic dataset, and moisture–depth profiles for the solar dry-back field experiments used in this comparison have been documented in Athmarajah et al. (2023), Athmarajah et al. (2024) and Athmarajah (2025). In the present study, the total energy required to remove 1 kg of water was calculated using an equivalent reference volume of 1 m × 1 m × 0.05 m. Under these conditions, the microwave convective drying system required approximately 0.3 – 0.5 MJ/kg of water removed, based on a combined microwave and convective power input of 2.9 kW over 4–6 min of drying. In contrast, solar dry-back over the same depth and reference volume required approximately 4–10 MJ/kg of water removed, depending on climatic conditions and drying duration. These results indicate that, within the surface layer, microwave convective drying is substantially more energy-efficient than solar drying, despite its higher instantaneous power demand and limited near-surface drying region. While this preliminary comparison offers an initial

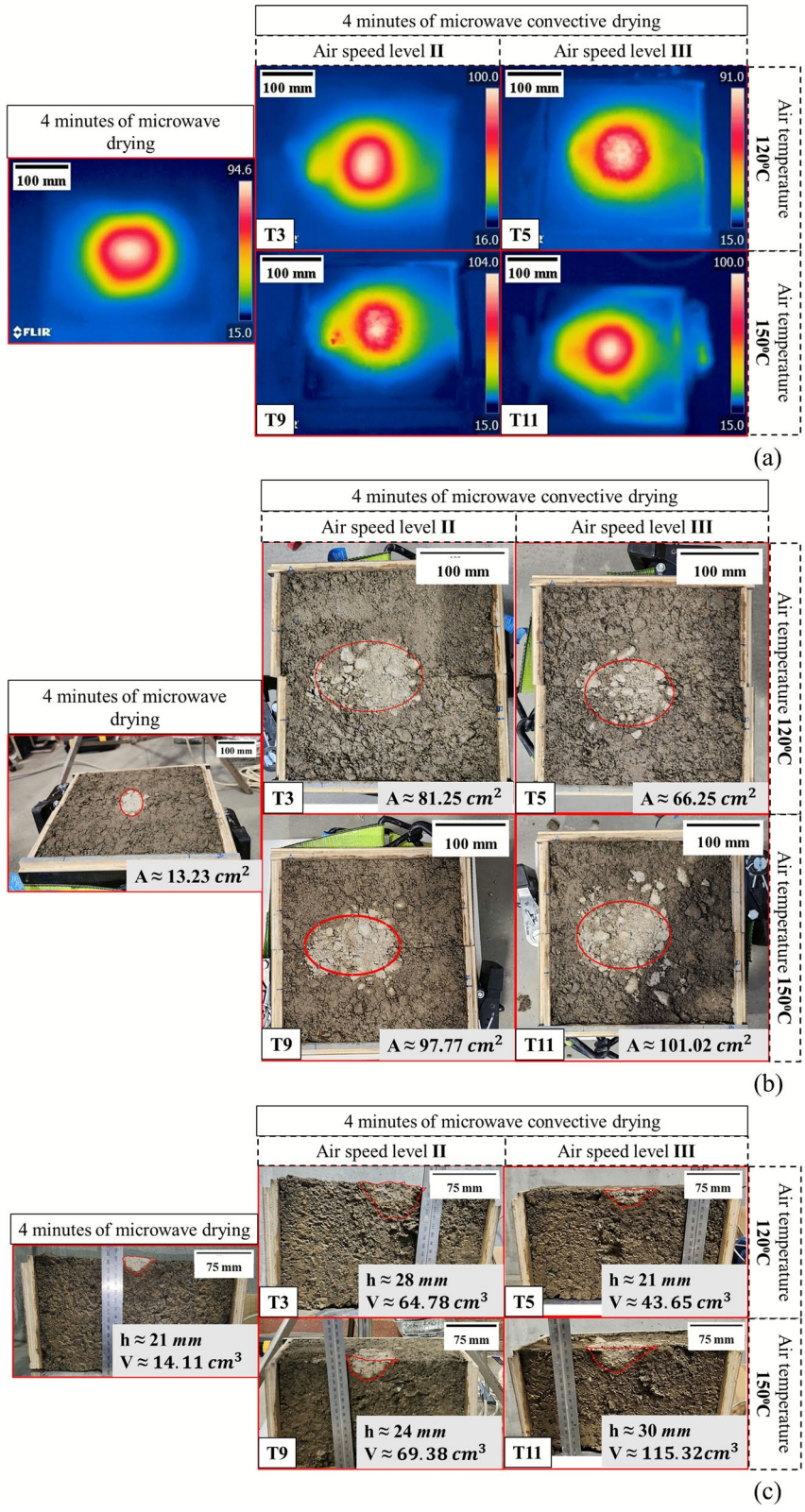

Fig. 13 Comparative analysis between microwave-only drying and microwave convective drying of compacted UGM samples after 4 min of drying: **a** IR thermal imaging, **b** Visible dried area at surface and **c** Visible dried region along the depth at centre

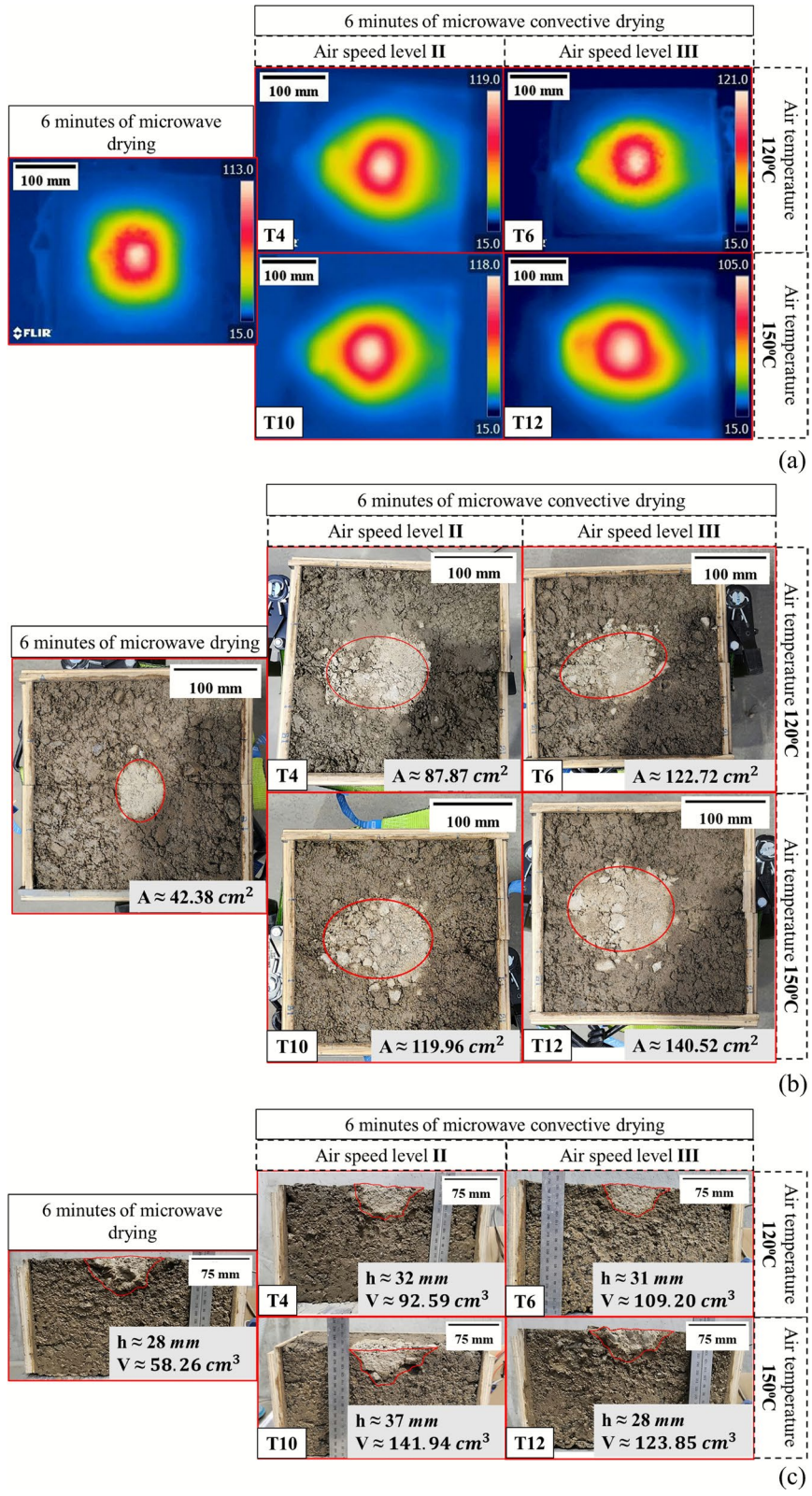

Fig. 14 Comparative analysis between microwave-only drying and microwave convective drying of compacted UGM samples after 6 min of drying: **a** IR thermal imaging, **b** Visible dried area at the surface, and **c** Visible dried region along the depth at centre

indication of the energy consumption of compacted UGM under microwave convective drying, further research is required to develop an energy-efficient and field-ready dry-back method. The energy values reported here are based on laboratory-scale experiments using a small-scale microwave applicator and a heat gun. The scalability of the proposed technique to real-world conditions, along with the associated sustainability, safety, and cost implications, has yet to be evaluated and remains a critical area for future investigation.

In practice, several strategies could be implemented to improve the feasibility of this technology. For instance, increasing microwave power, redesigning antenna configurations, and optimising convective airflow are potential avenues to enhance energy penetration. In addition, multi-pass or staged drying systems, similar to roller compaction, may also promote progressive drying of deeper layers. This approach is well established in microwave treatment of soils and food products, where intermittent heating cycles facilitate upward moisture migration between exposures, thereby enhancing overall drying efficiency (Vorhauer et al. 2019; Kumar et al. 2017; Khan et al. 2019). For large-scale applications, vehicle-mounted arrays of horn antennas with controlled hot airflow could operate in parallel to cover full lane widths, similar to multi-source microwave drying systems used in industrial processing (Brodie et al. 2019a; Gao et al. 2017). Use of lower microwave frequencies, such as 915 MHz, has also been reported to increase penetration depth in porous materials (Brodie et al. 2019b; Liao et al. 2024). Alternatively, the combined effect of microwave convective drying with conventional solar drying may increase the drying depth of the compacted granular pavement layers. Future improvements should therefore prioritise pilot-scale trials to evaluate these strategies and assess the energy efficiency, safety, cost, and overall practicality of microwave convective drying in large-scale road construction.

4.7 Parametric Study and Variable Importance Analysis

A parametric study was conducted using the trained machine learning models: SVM and GPR, to systematically investigate the influence of individual input parameters on the predicted drying behaviour of compacted UGM. This approach enabled a structured evaluation of variable sensitivity within the tested range of experimental conditions. In the analysis, one input variable was varied at a time while the remaining variables were held constant at their mean values according to the methodology of Kiani et al. (Kiani et al. 2016). Within the tested range, a parametric study was conducted to explore new combinations of drying conditions that had not been experimentally tested, providing additional insights without requiring further laboratory work.

Variable importance (VI), often referred to as sensitivity analysis, evaluates the effect of each input parameter on the model's output. This approach provided insights into the contribution of each input parameter to the predictive performance of the machine learning model. In this study, the sensitivity of a given input parameter (i) was determined by assessing the variation in model output (L_i) when the input parameter was varied from its maximum (i_{max}) to its minimum (i_{min}) value, while the other input parameters were kept constant at their mean values such that (Tophel et al. 2023a, 2025; Kiani et al. 2016).

$$L_i = \left| f\left(i_{\max}\right) - f\left(i_{\min}\right), \right| \tag{8}$$

where $f\left(i_{max}\right)$ and $f\left(i_{min}\right)$ are the model outputs when the input parameter i is set to its maximum and minimum values, respectively. The VI for each parameter was expressed as a percentage of its contribution to the total output variation, as calculated by

$$VI = \frac{L_i}{\sum_{j=1}^{j=n} L_i} \tag{9}$$

The results of the parametric study and variable importance analysis of each input variable at different depths from the material surface are shown in Fig. 15 and Fig. 16, respectively. Accordingly, Fig. 15a indicates that higher initial S_r led to higher final S_r across all depths, suggesting that compacted UGMs with higher initial S_r retain more moisture after drying. This effect is more pronounced at deeper layers, where moisture removal is slower due to limited energy penetration and reduced evaporation rates. The sensitivity analysis shown in Fig. 16a further supported this observation, showing that initial S_r had an increasing influence with

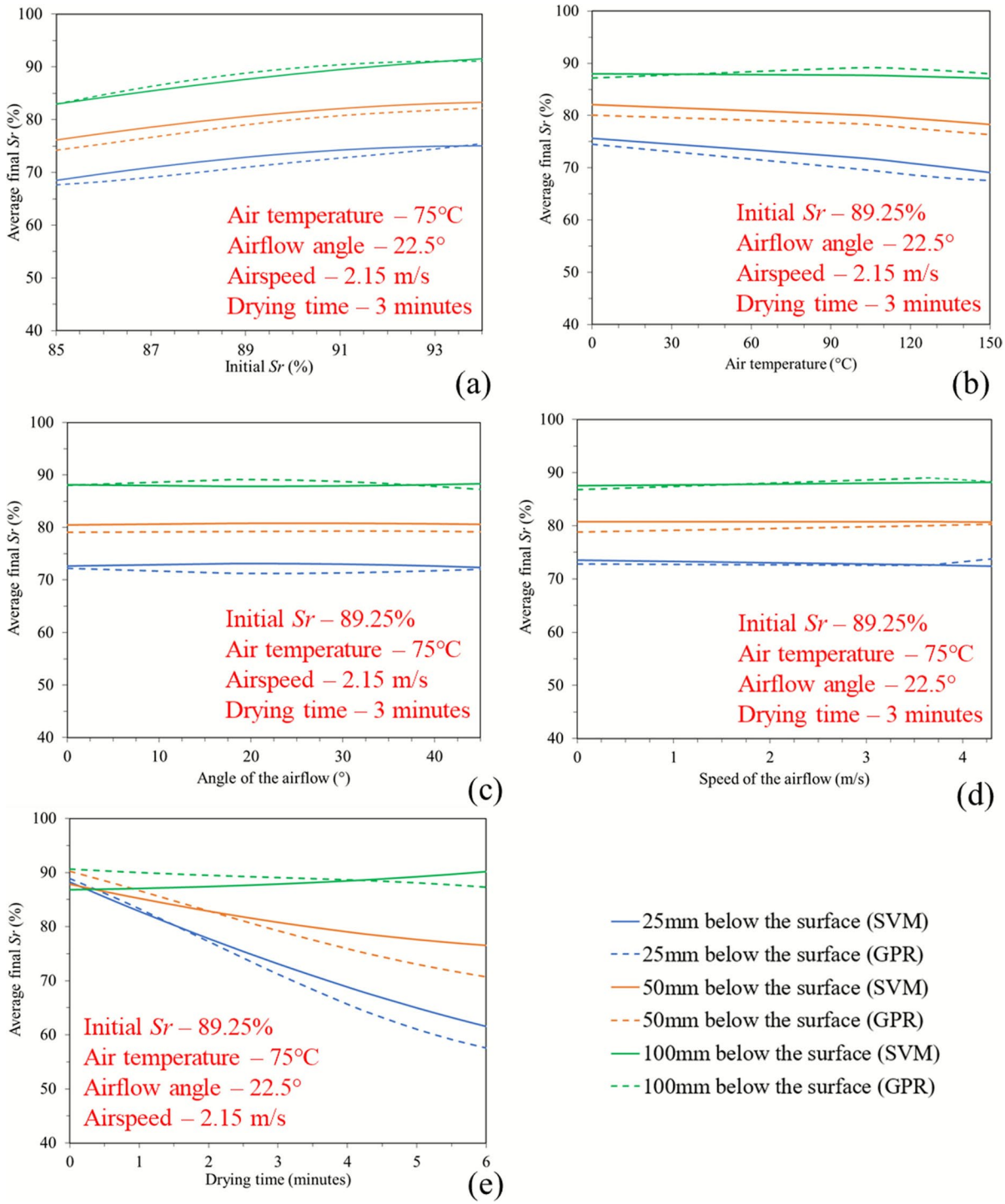

Fig. 15 Parametric study showing the variation of average S_r after drying with respect to each input variable at different depth from the surface: **a** Initial S_r, **b** Air temperature, **c** Angle of the airflow, **d** Speed of the airflow, and **e** Drying time

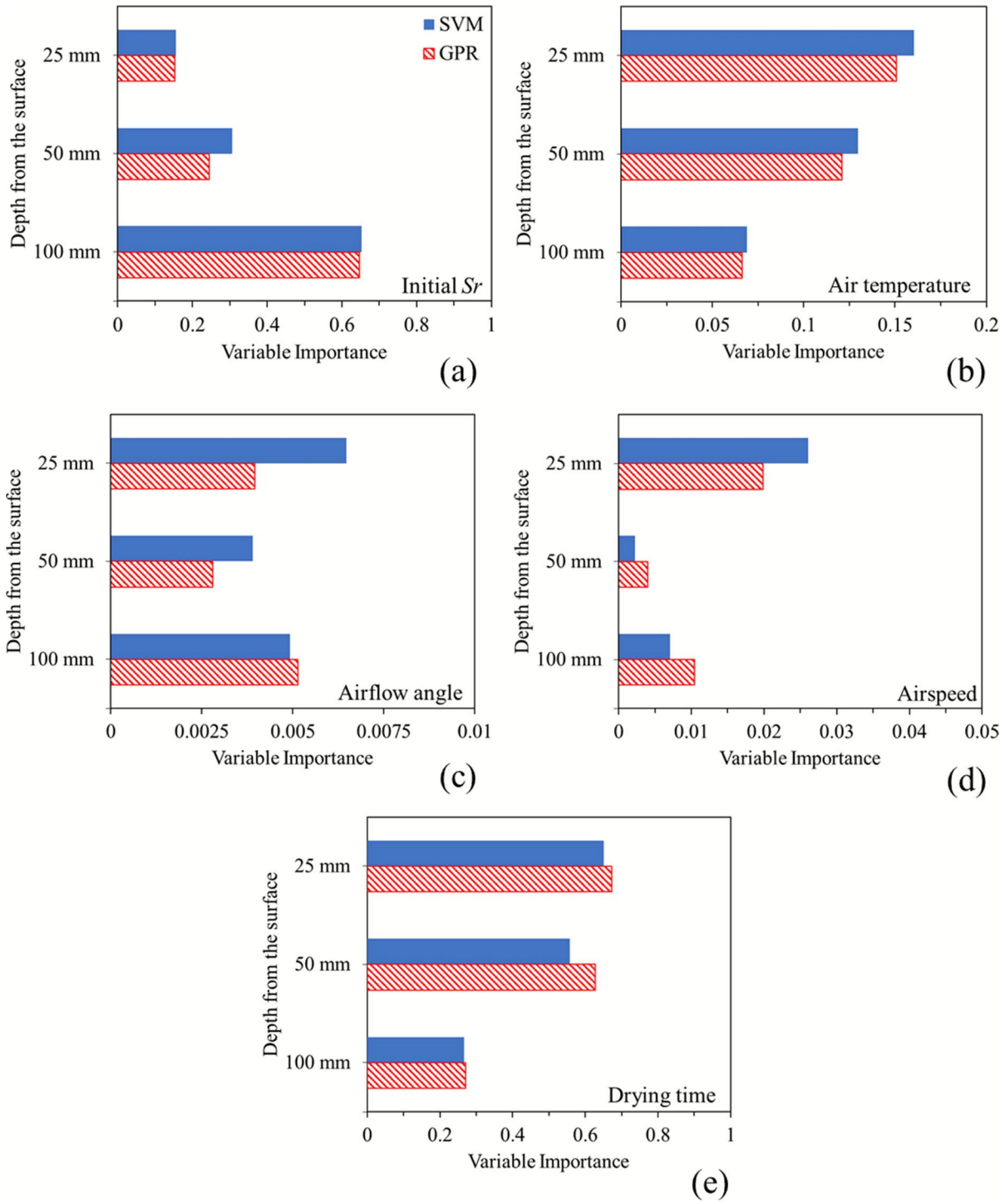

Fig. 16 Variable importance of each input parameter on the variation of average S_r (after drying) at different depths from the surface: **a** Initial S_r, **b** Air temperature, **c** Angle of the airflow, **d** Speed of the airflow, and **e** Drying time

depth. Near the material's surface, water movement was primarily driven by evaporation and capillary rise. At deeper depths, however, gravitational drainage governs redistribution, and water movement depends on hydraulic conditions due to the absence of strong evaporative forces (Ochsner et al. 2019). High initial S_r reduces matric suction and weakens capillary forces, thereby limiting hydraulic gradients and moisture migration within the sample, making initial moisture a critical factor in drying response (Castillo et al. 2015).

Increasing air temperature showed a noticeable variation in the average S_r (Fig. 15b), especially at a shallower depth (25 mm), indicating enhanced surface drying. The variable importance of air temperature also confirmed that the importance diminished with depth, as presented in Fig. 16b. Further, the higher airflow angle and increased airspeed depicted in Fig. 15c and Fig. 15d, respectively, did not show a substantial variation in the final S_r across all depths. Besides, the sensitivity of both airflow angle and airspeed was higher at surface levels, particularly at 25 mm depth, resulting in improved drying efficiency near the surface of the material. However, airflow angle had a reduced influence compared to other input features across all depths, as shown in Fig. 16. These trends are consistent with convective heat- and mass-transfer theory, as air temperature, airflow angle, and airspeed primarily influence surface moisture removal, while their effects diminish rapidly with depth due to the limited penetration of airflow and heat into the compacted UGM (Khan et al. 2022).

Figure 15e demonstrates that drying time is another critical factor, leading to a progressive reduction in S_r across all depths. Unlike other parameters, drying time had a consistent impact at both shallow and deeper depths, suggesting that prolonged exposure to microwave energy combined with hot airflow facilitated moisture to migrate from deeper layers. Extended drying times increase internal vapour generation and enhance vapour pressure gradients, which are the dominant driving forces for moisture transport during microwave convective drying (Kumar et al. 2017). Figure 16e confirmed this, ranking drying time as the most important factor across all depths. This emphasised that longer drying durations are crucial for enhancing moisture removal over depth, making it the most effective parameter in the drying process.

Overall, the parametric study and variable importance analyses were mostly aligned, showing that drying time and initial S_r were the dominant factors influencing the drying efficiency of the compacted UGM samples under microwave convective drying. At 25 mm depth, initial S_r and air temperature exhibited nearly the same importance (around 0.15), but their influence diverged with depth. Initial S_r became more dominant at greater depths (~0.65 at 125 mm), while air temperature decreased in importance to ~0.07 at the same depth. This result indicates that temperature mainly affects surface drying, while initial moisture conditions dictate deeper moisture retention. In contrast, while airflow angle and speed showed minor surface drying improvements in the parametric study, their overall influence on drying efficiency remained

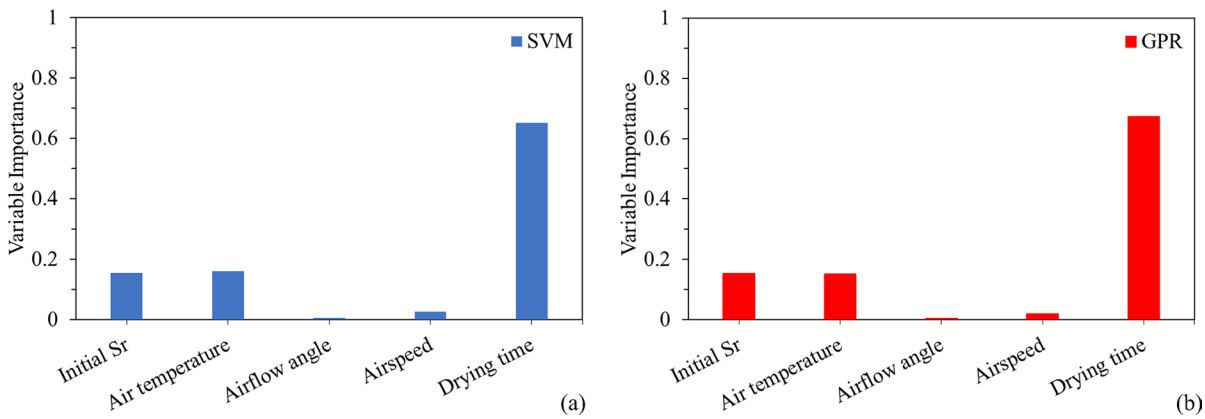

Fig. 17 Variable importance of input variables on the final S_r variation at a depth of 25 mm based on two different machine learning models: **a** SVM and **b** GPR

low in the variable importance analysis. These findings suggest that convective parameters were limited to surface drying, reinforcing the need for an optimisation process to improve drying uniformity.

Figure 17 illustrates the impact of all factors on the final S_r variation at a depth of 25 mm based on the SVM (Fig. 17) and GPR (Fig. 17b) models. The comparison at 25 mm depth was selected because the parametric study and variable importance analysis of each input feature at the different depths depicted in Fig. 15 and Fig. 16 indicate that air temperature, airflow angle, and airspeed had more influence at shallower depths. Both the SVM and GPR models agree that drying time was the dominant factor, with an importance value of approximately 0.65 in SVM and 0.67 in GPR, confirming that drying time played the most important role in influencing moisture removal efficiency. Initial S_r was the second most important factor, with a variable importance value of around 0.16 in SVM and 0.15 in GPR. This aligns with previous findings, indicating that higher initial S_r results in greater moisture retention after drying. However, its variable importance was substantially lower than drying time, highlighting that time-dependent moisture migration plays a greater role than initial moisture conditions at this depth.

Interestingly, despite the experimental results showing no major differences in final S_r with variations in air temperature, both models exhibited a noticeable level of importance for this variable (~0.16 in SVM and 0.15 in GPR), being slightly higher than the initial S_r in the SVM model. Alternatively, airflow angle and airspeed showed minimal importance in both models, with values below 0.05, confirming that these parameters have a negligible impact on drying efficiency at 25 mm depth.

While the machine learning models highlighted drying duration as the dominant parameter at all depths, they also identified initial S_r and air temperature as influential variables, particularly near the surface. However, caution must be exercised in interpreting these variable-importance results due to the small dataset size, which may limit their robustness and generalisability. Future studies should therefore further investigate the roles of these variables with larger datasets and consider validation techniques to improve model reliability.

5 Conclusion

This study investigated the efficiency and effectiveness of microwave convective drying of compacted unbound granular material (UGM) used in pavement construction through a limited number of controlled laboratory experiments. Comparative analyses were conducted with microwave drying to evaluate potential improvements in drying uniformity and surface moisture removal. The experimental results demonstrated that microwave convective drying substantially enhanced surface drying efficiency, increasing the dried surface area when compared to microwave drying alone. However, it was observed that effectiveness of moisture removal decreased markedly with depth, limiting the drying effect to approximately 30–50 mm. This poses a significant constraint for applying microwave convective drying in standard pavement layers, which exceed 75 mm in thickness. The limited depth of moisture removal was attributed to the constrained penetration of microwave energy and the surface-focused nature of convective heating.

To supplement the experimental findings and investigate parameter sensitivity, machine learning models, including the Support Vector Machine (SVM) and Gaussian Process Regression (GPR) were developed using the available experimental dataset, as these two models are better for small datasets compared to other machine learning models. Both models demonstrated promising predictive performance, with GPR showing particularly high accuracy (mean absolute error, MAE = 0.006%). However, the predictive capability of these models is limited to the specific UGM type, compaction state, and microwave–convective drying setup represented in this study, and their use outside these conditions is limited. Therefore, future research should validate and expand these models using larger and more diverse datasets to assess their robustness, improve generalisability across broader experimental conditions, and reduce concerns related to potential overfitting.

The study identified drying duration as the most critical parameter influencing moisture removal across different depths. Parameters such as hot air temperature, airflow angle, and airflow speed primarily influenced surface drying, with minimal impact on deeper moisture removal. Given these findings, future research should focus on strategies to enhance deeper penetration of microwave energy and improve

uniformity in moisture extraction. Possible avenues include adjustments in microwave power intensity, antenna design, or hybrid drying strategies that combine microwave convective drying with other technologies.

Due to the labour-intensive nature of sample preparation, compaction, and testing, experimental repetitions were not performed, and the number of test conditions per variable was limited. Although consistent procedures were followed, manual setup and measurement constraints may have introduced variability. Repeated trials under identical conditions are therefore recommended in future work to better quantify experimental uncertainty and confirm parameter sensitivities. Moreover, further work should also explore translating laboratory-scale results to field conditions, including pilot-scale studies under realistic construction scenarios. Lastly, this study did not assess the economic and environmental viability of microwave convective drying, being critical considerations for broader adoption. Future research should thus investigate these factors, evaluating energy consumption, operational costs, and sustainability in comparison to traditional drying practices.

In conclusion, while this study was preliminary in nature, it provides essential insights into the benefits and challenges of microwave convective drying for a compacted UGM. The method showed promise as an accelerated drying technique, particularly for surface layers or thin pavement layers. However, potential challenges remain regarding deeper moisture removal, practical scalability, and cost-effectiveness. Addressing these aspects in future research is essential to determine the feasibility and potential benefits of adopting this novel drying approach in pavement construction in a real field application.

Acknowledgements This research was part of a project (Project number: IH18.03.8) sponsored by the SPARC Hub (https://sparchub.org.au) within the Department of Civil Engineering, Monash University, funded by the Australian Research Council (ARC) Industrial Transformation Research Hub (ITRH) Scheme (Project ID: IH180100010). The financial and in-kind support of EIC Activities of CIMIC Group and Monash University are gratefully acknowledged, along with the financial support of the ARC. Special thanks are also extended to Professor Graham Brodie for generously providing the equipment (small-scale microwave applicator) used during the experimental work.

Author Contributions G.A. and A.T. performed the experiments and prepared the initial manuscript text. J.W. and J.K. supervised the project, provided resources and critical intellectual input, and reviewed and edited the final manuscript. All authors reviewed and approved the manuscript.

Funding This study was supported by the Australian Research Council (ARC) Industrial Transformation Research Hub (ITRH) Scheme (GrantNo. IH180100010).

Data Availability The data will be available upon reasonable request from the corresponding author.

Declarations

Conflict of Interest The authors declare no competing interests.

References

Arif A, Zhang C, Sajib MH et al (2025) Rock slope stability prediction: a review of machine learning techniques. Geotech Geol Eng 43(3):124

AS-1289.3.1.1, 2009 Soil classification tests - Determination of the liquid limit of a soil- Four point casagrande method. Standards Australia.

AS-1289.3.5.1 (2006) Methods of testing soils for engineering purposes - Soil classification tests - Determination of the soil particle density of a soil - Standard method. Standards Australia

AS-1289.3.6.1 (2009) Methods of testing soils for engineering purposes - Soil classification tests - Determination of the particle size distribution of a soil - Standard method of analysis by sieving. Standards Australia.

AS-1289.5.2.1 (2017) Methods of testing soils for engineering purposes - Soil compaction and density tests - Determination of the dry density/moisture content relation of a soil using modified compactive effort. Sydney: Standards Australia.

Athmarajah G (2025) *Microwave dry-back of granular pavement layers.* (Doctor of Philosophy). Monash University.

Athmarajah G, Sounthararajah A, Walker JP et al (2024) An alternative technology using microwaves for dry back process of unbound granular pavements during construction – a review. Transp Geotech. https://doi.org/10.1016/j.trgeo.2024.101245

Athmarajah G, Walker J, Chen L et al (2025) In Press. Microwave dry-back of compacted unbound granular materials - An experimental and numerical study. Géotechnique

Athmarajah G, Walker J P, Sounthararajah A, et al. 2023. Influence of solar energy on the dry back process in road pavement construction: An experimental study. XXVII PIARC World Road Congress, 11

Australian Radiation Protection and Safety Agency, A (2002) Maximum Exposure Levels to Radiofrequency Fields-3 kHz to 300 GHz

Austroads (2019) Guide to Pavement Technology Part 2: Pavement Structural Design

Awad M, Khanna R (2015) Support Vector Regression. Apress, Berkeley, CA, pp 67–80

Brodie G (2005) Microwave Timber Heating and its Application to Solar Drying. (Doctor of Philosophy). University of Melbourne

Brodie G, Khan M J and Gupta D (2019a) Microwave Soil Treatment and Plant Growth. *Sustainable crop production*

Brodie G, Pchelnikov Y, Torgovnikov G (2019b) Experimental study of microwave slow wave comb applications for timber treatment at frequencies 2.45 and 0.922 GHz. J Mater Sci Eng Adv Technol 17(2):63–90

Brodie G, Pchelnikov Y, Torgovnikov G (2020) Development of microwave slow-wave comb applicators for soil treatment at frequencies 2.45 and 0.922 GHz (theory, design, and experimental study). Agriculture. https://doi.org/10.3390/agriculture10120604

Castillo A, Castelli F, Entekhabi D (2015) Gravitational and capillary soil moisture dynamics for distributed hydrologic models. Hydrol Earth Syst Sci 19:1857–1869

Chaure A, Behera AK and Bhattacharya S (2023) Gaussian process regression for climate modeling: potentials, limitations, and advances in emulation techniques. *J Emerg Technolog Innov Res (JETIR)* 10(5)

Cristianini N, Shawe-Taylor J (2000) An introduction to support vector machines and other kernel-based learning methods. Cambridge University Press, Cambridge

Dai X, Andani HT, Alizadeh A a, et al (2023) Using Gaussian Process Regression (GPR) models with the Matérn covariance function to predict the dynamic viscosity and torque of SiO_2/Ethylene glycol nanofluid: A machine learning approach. *Eng Appl Artificial Intelligence* 122

Deb S, Chandra Pradhan R, Subbarao PMV et al (2024) Convective Drying. In: Gangawane KM, Dwivedi M, Chandra Pradhan R (eds) Advanced Computational Approaches for Drying in Food Processing. Springer International Publishing, Cham, pp 75–104

Department of Transport and Main Roads Queensland (2021) MRTS05-Unbound Pavements

Domínguez JM (2011) Drying. *Comprehensive Biotechnology* 727–735

Dutta TT, Tophel A and Kodikara J (2024) Resilient and rutting response of unbound granular material and subgrade soil influenced by initial state and stress conditions. *Road Mater Pavement Des* 1–33

Elsawy MBD, Alsharekh MF, Shaban M (2022) Modeling undrained shear strength of sensitive alluvial soft clay using machine learning approach. Appl Sci 12(19):10177

FLIR Systems 2009 User Manual. In: Systems, F. ed

Gao J, Sha A, Wang Z et al (2017) Utilization of steel slag as aggregate in asphalt mixtures for microwave deicing. J Clean Prod 152:429–442

Griffin, J (2015) P11 Review of Unbound Pavement Material Specifications: Wet/Dry Strength Variation (Year 1 – 2013/14 and Year 2 – 2014/15).

Himanshu K, Vipul DP, Girish KJ (2010) Microwave Technology-A potentential tool in pharmaceutical science. Int J PharmTech Res 2:1754–1761

Izli G, Yildiz G, Berk SE (2022) Quality retention in pumpkin powder dried by combined microwave-convective drying. J Food Sci Technol 59(4):1558–1569

Khan MIH Batuwatta-Gamage C P, Karim M A, et al (2022) Fundamental Understanding of Heat and Mass Transfer Processes for Physics-Informed Machine Learning-Based Drying Modelling. *energies,* 15

Khan MJ, Brodie G, Gupta D (2019) Potential of microwave soil heating for weed management and yield improvement in rice cropping. Crop Pasture Sci 70(3):211–217

Kiani B, Gandomi AH, Sajedi S et al (2016) New formulation of compressive strength of preformed-foam cellular concrete: an evolutionary approach. J Mater Civ Eng 28(10):04016092

Kodikara J, Islam T, Sounthararajah A (2018) Review of soil compaction: history and recent developments. Transp Geotech 17:24–34

Kukkapalli VM and Pulugurtha SS (2018) Effect of road construction projects on travel time reliability. *Int Conf Transport Develop* 45–56

Kumar C, Joardder MUH, Farrell TW et al (2017) Investigation of intermittent microwave convective drying (IMCD) of food materials by a coupled 3D electromagnetics and multiphase model. Drying Technol 36(6):736–750

Li B, Feng S, He Q et al (2024) Numerical simulation of continuous microwave drying of rice grains. J Food Process Eng. https://doi.org/10.1111/jfpe.14678

Li P, Ma C, Chen Z et al (2023) A review: study on the enhancement mechanism of heat and moisture transfer in deformable porous media. Processes. https://doi.org/10.3390/pr11092699

Liao C, He Z, Tang R et al (2024) The research on microwave drying characteristics of polyethylene terephthalate materials based on frequency and power tuning technology. Processes 12(7):1488

Maha Madakalapuge C, Dutta TT, Kodikara J (2024) Evaluation of climatic effects on moisture variation and performance of unbound pavements with sprayed seals. Acta Geotech 19(8):5481–5502

Malafronte L, Lamberti G, Barba AA et al (2012) Combined convective and microwave assisted drying: experiments and modeling. J Food Eng 112(4):304–312

Midgley L (2010) Technical Report TR 209 Best Practice for the Preparation of New Granular Pavement for Thin Bituminous surfacing.

Mountrakis G, Im J, Ogole C (2011) Support vector machines in remote sensing: a review. ISPRS J Photogramm Remote Sens 66(3):247–259

Ochsner TE, Howerton E and Ellis B (2019) Rain or Shine: An Introduction to Soil Physical Properties and Processes. Oklahoma State University Libraries

Ouertani S, Hassini L, Azzouz S et al (2015) Modeling of combined microwave and convective drying of wood: prediction of mechanical behavior via internal gas pressure. Drying Technol 33(10):1234–1242

Pan Y, Yang C, Zhang L (2025) Rapid estimation of rock mass mechanical properties using machine learning and wave velocity. Geotech Geol Eng 43(5):216

Rajewska K and Pawłowski A (2018) Application of microwaves in the convective drying of ceramic. Proceedings of 21th International Drying Symposium

Rasmussen CE, Williams CKI (2006) Gaussian Processes for Machine Learning. MIT Press

Salour F (2015) Moisture influence on structural behaviour of pavements - Field and laboratory investigations. Doctoral Thesis (Doctor of Philosophy). Royal Institute of Technology (KTH)

Sangsefidi E, Wilson DJ, Larkin TJ et al (2019) The role of water in unbound granular pavement layers: a review. Transp Infrastruct Geotechnol 6(4):289–317

Shao W, Yue W, Zhang Y et al (2023) The application of machine learning techniques in geotechnical engineering: a review and comparison. Mathematics 11(18):3976

Smola AJ, Schölkopf B (2004) A tutorial on support vector regression. Stat Comput 14(3):199–222

Sousa LHCD, Motta Lima OC, Pereira NC (2006) Analysis of drying kinetics and moisture distribution in convective textile fabric drying. Drying Technol 24(4):485–497

Sun J, Oh E, Ong DE-L (2021) Influence of degree of saturation (DOS) on dynamic behavior of unbound granular materials. Geosciences. https://doi.org/10.3390/geosciences11020089

Tophel A, Dutta TT, Otsubo M, et al (2023a) Machine learning models to estimate stress wave velocities of cohesionless soils during triaxial compression influenced by particle characteristics. *Soil Dynam Earthquake Eng* 165

Tophel A, Nguyen TM, Walker JP et al (2025) Soil moisture prediction in pavement layers using LSTM neural networks. Geotech Geol Eng 43(6):318

Tophel A, Walker J P, Dutta TT, et al (2023b) Model development to Predict Dynamic Interactions of Roller and Geomaterial using Simulated Roller Compaction. *Transportat Geotech,* 39

Tuffour HO, Bonsu M, Atakora WK et al (2014) Evaporative cooling of wet soil surface under different agricultural land use systems. Int J Sci Res Environ Sci 2(9):323–331

Ulloa RZ, Santiago MGH and Rueda VLV (2019) The Interaction of Microwaves with Materials of Different Properties. In: Kim Ho, Y. and Kazuhiro, H. eds. *Electromagnet Fields Waves.* Rijeka: IntechOpen, Ch. 6

VicRoads (2017) Code of Practice RC 500.02 - Registration of Crushed Rock Mixes. 9

Vorhauer N, Tretau A, Bück A et al (2019) Microwave drying of wet clay with intermittent heating. Drying Technol 37:667–678

Williams CKI, Rasmussen CE (1996) Gaussian processes for regression. Adv Neural Inform Process Syst (NIPS) 8:514–520

Yao L, Song Z, Sun C et al (2020) Study on the evolution of internal and external water of lignite during microwave drying and the moisture reabsorption characteristics of dried lignite. *Energ Sour, Part A: Recov, Utilizat Environmental Effects* 1–18

Zhang P, Yin Z-Y, Jin Y-F et al (2022) Modelling the mechanical behaviour of soils using machine learning algorithms with explicit formulations. Acta Geotech 17(4):1403–1422